Thesis for the degree of Licentiate of Engineering

Radially global neoclassical transport in tokamak pedestals

Stefan Buller

CHALMERS

Department of Physics
Chalmers University of Technology
Göteborg, Sweden, 2017

Radially global neoclassical transport in tokamak pedestals
Stefan Buller

Technical Report No. CTH-NT-331
ISSN 1653-4662
Subatomic and Plasma Physics
Department of Physics
Chalmers University of Technology
SE–412 96 Göteborg
Sweden
Telephone +46–(0)31 772 1000

Some figures in this thesis are in color only in the electronic version, available online through Chalmers Publication Library.

Cover:
A streamplot of particle fluxes in the radial-poloidal plane, for deuterium plasma with a helium impurity in a tokamak pedestal.

Printed in Sweden by
Reproservice
Chalmers Tekniska Högskola
Göteborg, Sweden, 2017

Radially global neoclassical transport in tokamak pedestals

Stefan Buller
Department of Physics
Chalmers University of Technology

Abstract

Nuclear fusion has the potential to become a sustainable energy source in the foreseeable future. The most developed system for fusion power production is the tokamak, which magnetically confines a plasma at high enough temperature for fusion reactions to take place.

Tokamaks operating in the H-mode feature the largest known steady state density and temperature gradients, located in a region at the edge of the plasma known as the *pedestal*. These steep gradients result from a spontaneous reduction in turbulence, and as a result of these steep gradients, the plasma behavior couples between nearby radial locations, and can no longer be evaluated in terms of plasma parameters at a single radius. The plasma behavior is said to be *radially global*. This makes it challenging to model the transport of particles, heat, etc., which is needed to design and evaluate future reactors.

In this thesis, we study collisional, radially-global transport in tokamak pedestals, using numerical methods to solve a drift-kinetic equation for the distribution of particles in both velocity and configuration space. Particular focus is put on the influence of non-trace impurities, and the effects of changing the mass and charge of the bulk ions. Order unity deviations from radially-local results are observed in plasma flows and cross-field fluxes, both in the pedestal and the near-pedestal core. In addition, a significant radial transport of angular momentum arises in the radially-global description, which may have implications for the plasma rotation, which is understood as a crucial component for the transition to H-mode.

Keywords: fusion, tokamak, plasma physics, transport, collisional transport, drift-kinetics, global effects

Publications

[A] I. Pusztai, S. Buller, and M. Landreman, *Global effects on neoclassical transport in the pedestal with impurities*, Plasma Physics and Controlled Fusion **58**, 085001 (2016).
https://doi.org/10.1088/0741-3335/58/8/085001

[B] S. Buller, I. Pusztai, and M. Landreman, *Neoclassical transport with non-trace impurities in density pedestals*, Europhysics Conference Abstracts **40A**, O4.118 (2016).
http://ocs.ciemat.es/EPS2016PAP/pdf/O4.118.pdf

[C] S. Buller, I. Pusztai, S.L. Newton, and J.T. Omotani, *Neoclassical flows in deuterium-helium plasma density pedestals*, Plasma Physics and Controlled Fusion **59**, 055019 (2017).
https://doi.org/10.1088/1361-6587/aa658a

[D] S. Buller and I. Pusztai, *Isotope and density profile effects on pedestal neoclassical transport*, Plasma Physics and Controlled Fusion **59**, 105003 (2017).
https://doi.org/10.1088/1361-6587/aa7e5c

Contents

Acknowledgments

There are a lot of things that go into producing a thesis, and educating a PhD student.

Thanks to István Pusztai for being an excellent supervisor, for teaching me how to research, how to do plasma physics, for his help proofreading this manuscript and for bearing with me. None of the work in this thesis would be the same without him, and the list of things I am grateful for could probably fill a thesis of its own, so I will just say: thanks for everything.

Also thanks to my other supervisors, John Omotani and Sarah Newton, for all the helpful discussions on neoclassical theory, being PERFECT, life in general, and for their heroic efforts in proofreading this manuscript.

Also thanks to my parents – not for proofreading this manuscript – but for conceiving and raising me and my siblings, who I'm also grateful to for being fun to have around.

Also, thanks to my grandparents, for raising my parents (and me and my siblings), and so on.

Thanks to Tünde Fülöp for her enthusiastic guidance, and for leading the Chalmers Plasma Theory group with a keen eye for research (and other) opportunities for everyone.

Special thanks to Matt Landreman for writing the PERFECT code, and for his help and advice on how to run it.

Last but not least, I would like to thank the members of the Chalmers Plasma Theory group for filling my days with fruitful discussions (and occasional distractions), which make it even more enjoyable to work with plasma physics. An honorable mention goes to Tim Dubois, who, due to sharing an office with me, has provided the most numerous, not unwelcome, distractions.

Chapter 1

Introduction

As energy is conserved, every process – such as reading this text or even thinking – can be thought of as converting energy from one form to another. However, when energy is transferred within a system, it is typically redistributed over more parts of the system, until it is so thinly distributed that it can no longer be used to perform work. This result – the second law of thermodynamics – implies that useful energy ("free energy") is effectively consumed, and cannot be produced [1, 2].

Although we cannot create energy, we can extract it from systems which have yet to reach their minimum free energy. The most prominent everyday example of such a system is the Sun, which effectively acts as the battery of the entire solar system.

The source of the Sun's energy lies in the curious fact that the nuclear binding energy per nucleon increases for light atomic nuclei, so that energy can be extracted by merging lighter elements together – the process of *nuclear fusion*. The binding energy continues to increase until around ^{62}Ni, which is therefore the heaviest element that can be formed with a net energy gain [3–5]. Since roughly 75% (by mass) of the ordinary matter in the universe is hydrogen [6], it would seem that a vast amount of energy could potentially be extracted by fusion. However, the fact that the universe *is* mostly hydrogen also tells us that fusion does not happen easily: these nuclei have been firmly stuck in local free energy minima since the early eras of our universe.

The difficulty lies in the fact that atomic nuclei repel each other, so their energetically favorable union can only occur if their kinetic energy is sufficiently high to overcome the Coulomb barrier between them. To put things in perspective, a thermal particle at room temperature has

a kinetic energy around 25 meV, while an energy of about 0.1 MeV is required to take advantage of the maximum cross section of the reaction between deuterium and tritium isotopes [7, 8], the deuterium-tritium (D-T) reaction[1].

Despite the high energies required, fusion is regularly achieved in nuclear physics experiments with ion beams [9]. However, these experimental setups cannot be utilized as an energy technology. The fundamental problem is that beams thermalize due to Coulomb interactions at a much higher rate than fusion reactions occur, so that only a few initial head-on reactions can occur.

To counter such problems, the ions must be prevented from rapidly leaving the system, and must be energetic enough that their thermalized velocity distribution has a sufficiently large number of ions with high enough energies to achieve fusion. For terrestrial fusion, temperatures around one hundred million Kelvin are required [10], which is about 10 times hotter than the core of the Sun [11].

An attractive way to confine such a hot, ionized gas is to utilize magnetic fields – an approach known as *magnetic confinement fusion*. An ionized gas under these conditions is called a (magnetized) plasma. A plasma is a gas of charged particles which is dominated by collective – rather than single particle – effects. A plasma is said to be magnetized when the magnetic field is strong enough to dominate the particle dynamics, which essentially is a requirement for magnetic confinement.

When the plasma is confined, the fusion reactions themselves can potentially be used to maintain the temperature of the plasma. Consider the D-T reaction,

$$D + T \rightarrow {}^4\mathrm{He} + n + 17.6\,\mathrm{MeV}, \tag{1.1}$$

where energy and momentum conservation demands that 1/5 of the released energy (3.5 MeV) goes to the helium ion ^{4}He, and 4/5 (14.1 MeV) to the neutron n. Since the helium ions are charged, they will also be confined by the magnetic field, and can transfer their kinetic energy to the fuel. If the heating generated in this way is sufficiently large to compensate for the net energy flux from the fusing plasma, it can sustain itself for as long as it is refueled. In addition, if the losses are small enough so that little external heating is needed, net energy can be

[1] This is the easiest fusion reaction to extract energy from on Earth, due to the large amount of energy released in the reaction, its high cross-section at relatively "low" energies, and the abundance of fuel.

extracted from the system. The viability of a fusion power plant thus depends on achieving low heat losses, and hence we need a solid understanding of these losses in order to design and predict the behavior of such power plants.

One of the most promising magnetic confinement schemes for a fusion reactor is the *tokamak*. It is a toroidally symmetric device with a large, externally generated toroidal magnetic field, and a smaller poloidal field generated by currents in the plasma.

This thesis is concerned with modeling of the transport of heat, particles, and momentum in tokamak fusion plasmas. Specifically, we are concerned with transport in the sharp gradient region found near the edge of H-mode tokamak plasmas – a region known as *the pedestal*. The tokamak is introduced in more detail at the end of chapter 2; in the following section, we outline relevant details of the H-mode pedestal.

1.1 The High confinement mode

In order to achieve the hundred million Kelvin required in a magnetic fusion reactor on our cold planet, large temperature gradients need to be maintained. With larger gradients, the reactor can be made smaller and less expensive.

However, temperature gradients are sources of free energy, and naturally decay unless heating is provided. The rate at which this decay happens typically increases with the gradients. Large steady-state gradients thus either require large applied heating, or that the heat flux driven by the gradients somehow is made small. The former option is unattractive for a reactor, which should therefore be designed to minimize the heat transport.

Unfortunately, the heat transport in modern fusion experiments is frequently observed to be *stiff*, i.e. it increases rapidly once the gradient crosses some threshold known as a *critical gradient* [12–14]. The origin of this increase in transport can be attributed to the excitation of small-scale turbulent structures, which give rise to a sizable turbulent transport [15]. This turbulent transport effectively limits the gradients to the critical values, which thus implies a minimum size for a plasma with fusion relevant temperatures.

As larger reactors imply a larger capital cost, understanding and suppressing plasma turbulence would be a major step towards economically viable fusion power. In fact, turbulence is routinely suppressed in

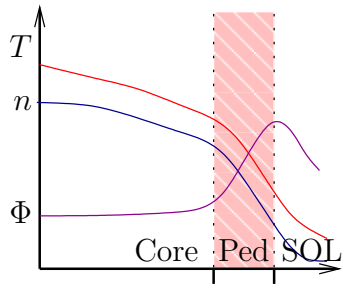

Figure 1.1: A cartoon of radial profiles of temperature T, density n and electrostatic potential Φ in the edge of an H-mode tokamak plasma, with core, pedestal ("Ped"), and Scrape-Off layer ("SOL") regions highlighted.

so-called *edge transport barriers* in fusion devices operated in the *high-confinement mode* [16, 17], often called simply the *H-mode*. The reduction in turbulent transport allows for sharp gradients to develop in the edge of these H-mode plasmas, a feature known as the *pedestal* [18]. This is illustrated in Figure 1.1, which schematically shows radial profiles of temperature (T), density (n), and the electrostatic potential (Φ) in the edge of an H-mode tokamak plasma, with different regions highlighted.

The sharp gradients in the pedestal will likely be useful to future fusion reactors: all current plans for magnetic fusion reactors feature at least an edge transport barrier [19, 20], and sometimes additional internal transport barriers [19]. These regions are also interesting to study theoretically, as the sharper gradients challenge some of the assumptions typically used to study transport in fusion plasmas. In the context of the core and pedestal transport, these assumptions may be stated as follows:

In the core region, the radial transport is predominantly turbulent and the gradients are thus limited. In this region the plasma profiles vary weakly over a particle orbit, which means that the transport can be described by a conventional *radially local* theory, in which the flux at a given radius can be described in terms of plasma parameters at that radius. The typical arguments used to derive a local theory can be sketched as follows: Confined particle orbits in tokamak magnetic fields are typically close to periodic. If a particle moves very little radially during its approximately periodic orbit, we can average over multiple orbits to obtain an effective force acting at the average radius of the

particle, r. To illustrate this, we expand a plasma profile X around r

$$X(r+\Delta r) = X(r) + \Delta r \left.\frac{\partial X}{\partial r}\right|_r + \mathcal{O}\left(\Delta r^2\right), \tag{1.2}$$

where Δr is the difference between r and the actual radial position of the particle. If the second term is small, $\Delta r \left.\frac{\partial X}{\partial r}\right|_r \ll X(r)$, only a low order approximation to Δr will be needed, so that we can approximate $X(r+\Delta r) \approx X(r)$ for the purpose of calculating Δr itself. This approximation yields a *radially local* description of the plasma, as the X felt by the particle over its orbit (1.2) can be expressed entirely in terms of the value and derivative(s) of X at r.

On the other hand, in the pedestal region ("Ped" in Figure 1.1), the profiles vary significantly over an orbit width, so that the derivative terms in (1.2) will not be small, and a local theory is not valid. This complicates the understanding of the H-mode, as the transport at a given radius r does not only depend on the plasma properties at r: the transport is *radially global*. It is this global transport that is the focus of this thesis.

Due to the radially global nature of the pedestal transport, it will also be affected by the outermost region depicted in Figure 1.1, the *scrape-off layer* ("SOL"). This is a comparatively sparse region located directly outside the confined region. Here, the magnetic field connects directly to the wall, so plasma is no longer confined. This region will not be treated in this thesis, but ought to be included in more complete pedestal models.

In general, the modeling presented in this thesis is not meant to be predictive of pedestal transport, as accounting for all the relevant processes (collisional and turbulent transport, instabilities, SOL physics – such as wall-plasma interactions, etc.) in a radially global setting is both conceptually and computationally extremely difficult. Instead, we study the reduced problem of collisional transport in a sharp gradient region, which is theoretically interesting as a simple model for investigating global effects, and experimentally relevant, as the pedestal transport is often found to be comparable to predictions of naive, radially local collisional transport models [21–25].

1.2 Thesis outline

The rest of this thesis is structured as follows. The upcoming chapters present the tokamak and tokamak transport: what an orbit width is,

how to formalize the above arguments, and finally a derivation of an equation which describes the radially global transport. In chapter 2, we introduce the basic concepts needed to describe how a tokamak confines the plasma. In chapter 3, we use these concepts to derive an equation for the distribution function in the pedestal and the core. This equation was originally derived by Kagan & Catto [26], although we follow the derivation due to Landreman [27] using the recursive drift-kinetic equation as derived by Hazeltine [28, 29]. Numerical solutions to this equation, obtained using the PERFECT code [27, 30], are the central results of this thesis. We also relate the distribution function to the fluxes of heat, particles and momentum. In the final chapter, chapter 4, the results of our studies on the effects of plasma composition and impurities (non-fuel plasma species) on the pedestal transport are summarized. These results are presented in detail in the included papers.

Chapter 2

Tokamak basics

In this chapter, we describe the basic concepts underlying most of magnetic fusion research, including the work done in this thesis. We start by describing single particle orbits in constant magnetic fields, which provides a simple example of how magnetic fields can be used to confine a particle. In this context, we introduce the concept of the guiding-center, which is then used to derive approximate solutions to the equations of motion in more general fields, allowing us to address the shortcomings of the constant field scenario and fully confine a particle. We then discuss how a particle is confined in the axisymmetric fields used in tokamaks, which is one of the central results needed as a background to understand this thesis.

To describe a tokamak plasma – rather than just a single particle as above – the interactions between the plasma particles also need to be taken into account. In the last section of this chapter, we sketch a statistical approach for describing the evolution of a distribution of N-particles interacting via long-range Coulomb collisions, resulting in the Fokker-Planck equation that is fundamental to most kinetic descriptions of plasma.

These two results – the single particle motion and the Fokker-Planck equation – will be used to derive a radially-global drift-kinetic equation in chapter 3, from which we can calculate collisional particle, heat and momentum fluxes in the pedestal.

2.1 Magnetic confinement of a single particle

Magnetic confinement relies on the Lorentz-force to confine charged particles,

$$\boldsymbol{F} = e(\boldsymbol{E} + \boldsymbol{v} \times \boldsymbol{B}), \tag{2.1}$$

where $\boldsymbol{F}$ is the force acting on a particle with charge e, $\boldsymbol{v}$ is the particle velocity, $\boldsymbol{E}$ is the electric field, and $\boldsymbol{B}$ is the magnetic field. In general, the fields will depend on position and time – although we will not consider time variations in this thesis, as we ultimately want steady-state fusion reactors, and we do not study turbulent fluctuations. In addition, the charged particles themselves generate electromagnetic fields, which couple the dynamics of different particles and greatly complicate the problem.

As a starting point, we first consider the case of a single particle in a stationary, homogeneous $\boldsymbol{B}$ with $\boldsymbol{E} = 0$. In the direction perpendicular to the field (which we denote by a subscript $\perp$), the particle will circle a magnetic field-line with a radius given by the gyroradius $\rho = v_\perp/\Omega$, where $\Omega = eB/m$ is the gyrofrequency, m the particle mass, and $v_\perp$ its velocity perpendicular to the magnetic field. Specifically, the perpendicular motion is given by

$$\boldsymbol{x}_\perp = \boldsymbol{C} + \boldsymbol{\rho}, \tag{2.2}$$

$$\boldsymbol{v}_\perp = v_\perp[\boldsymbol{e}_1 \cos(\Omega t) - \boldsymbol{e}_2 \sin(\Omega t)] \equiv v_1 \boldsymbol{e}_1 + v_2 \boldsymbol{e}_2, \tag{2.3}$$

where $\boldsymbol{e}_1, \boldsymbol{e}_2$ are unit-vectors that form an orthonormal basis together with $\boldsymbol{b}$, the unit vector in the $\boldsymbol{B}$ direction; $\boldsymbol{C}$ is a constant vector that depends on the initial conditions. The gyrovector, $\boldsymbol{\rho}$, is the time-integral of $\boldsymbol{v}_\perp$, and can thus be written

$$\boldsymbol{\rho} = \rho[\boldsymbol{e}_1 \sin(\Omega t) + \boldsymbol{e}_2 \cos(\Omega t)] = \frac{\boldsymbol{b} \times \boldsymbol{v}_\perp}{\Omega}. \tag{2.4}$$

As time evolves, only the *gyrophase*,

$$\gamma = \Omega t = -\arctan \frac{v_2}{v_1}, \tag{2.5}$$

changes, and the particle is thus confined within a radius ρ in the direction perpendicular to the magnetic field. This is the basis of magnetic confinement.

However, in the direction parallel to the magnetic field (which we denote by a subscript $\|$), the particle moves with a constant velocity, $v_\|$, and is thus unconfined.

If we add a constant force $\boldsymbol{F}$ to the constant magnetic field case – due to, for example, a constant electric field – the particle will accelerate indefinitely due to any component of $\boldsymbol{F}$ parallel to $\boldsymbol{B}$. Any perpendicular component $\boldsymbol{F}_\perp$ will cause the particle to execute an additional *drift motion* perpendicular to the magnetic field

$$\boldsymbol{v}_\mathrm{d} = \frac{\boldsymbol{F} \times \boldsymbol{B}}{eB^2}. \tag{2.6}$$

Hence the addition of a constant $\boldsymbol{F}$ causes the particle to drift away from the field-line, and thus does not confine it. For confinement, we therefore have to consider more general fields.

To prepare for the discussion of more general fields, we devote the remainder of this section to introducing the concept of the *guiding-center*. In magnetic fusion, it is often convenient to consider the position of the center of the gyrating motion – the guiding-center – rather than the particle position. There are numerous reasons for this: as shown in the following section, it will allow us to construct approximate analytical solutions for the motion in more general fields that remains accurate over times much longer than $1/\Omega$ [31, 32]; in simulations of particle orbits, it alleviates the burden of having to resolve the short time and length-scales associated with the gyrating motion [33]; finally, in kinetic theory, it allows for the elimination of the gyrophase γ as a phase-space coordinate, which reduces the dimensionality of the problem [34] – a result we will demonstrate in chapter 3.

We denote the guiding-center by $\boldsymbol{X}$, and define the *gyroaverage* of a quantity A as

$$\langle A \rangle_{\boldsymbol{X}} = \frac{1}{2\pi} \oint \mathrm{d}\gamma A(\boldsymbol{X}, v_\parallel, v_\perp, \gamma), \tag{2.7}$$

where $\boldsymbol{X}$, $v_\parallel$ and $v_\perp$ are kept fixed during the average. By definition, $\langle \boldsymbol{x} \rangle_{\boldsymbol{X}} = \boldsymbol{X}$, and it is trivial to show that $\langle \boldsymbol{\rho} \rangle_{\boldsymbol{X}} = 0$, $\langle \boldsymbol{v}_\perp \rangle_{\boldsymbol{X}} = 0$, and that $\boldsymbol{x} = \boldsymbol{X} + \boldsymbol{\rho}$, as required. The velocity of the guiding-center is given by $\dot{\boldsymbol{X}} = v_\parallel \boldsymbol{b} + \boldsymbol{v}_\mathrm{d}$, with $\boldsymbol{v}_\mathrm{d}$ given by (2.6) – again reflecting the fact that constant fields will not confine particles. Having rephrased this result in terms of the guiding-center, we are now ready to move on to considering magnetic fields with spatial variations.

Of particular interest are magnetic fields with weak variations, as this class of fields turns out to be sufficiently general to confine particles, and can be treated perturbatively in a manner that yields analytic expressions that remain accurate over reactor relevant time-scales. We consider single-particle motion in such fields in the following section.

2.1.1 Approximately constant fields

Small deviations from the constant field case can be accounted for perturbatively in the guiding-center formalism. If we assume that the magnetic field felt by the particle changes little during a gyration, we can view this change as a small perturbation and use it to calculate corrections to the motion in the homogeneous field.

To see this, we expand the magnetic field around the guiding-center $\boldsymbol{X}$:

$$\boldsymbol{B}(\boldsymbol{x}) = \boldsymbol{B}(\boldsymbol{X}+\boldsymbol{\rho}) = \boldsymbol{B}(\boldsymbol{X}) + \boldsymbol{\rho}\cdot\nabla\boldsymbol{B}(\boldsymbol{X}) + \mathcal{O}\left(\rho^2\right). \tag{2.8}$$

Here, we take $\boldsymbol{x} = \boldsymbol{X}+\boldsymbol{\rho}$, which is only exact in the constant field case, but is sufficient for our present purposes, as we will see[1].

If the magnetic field changes little on the gyroradius scale, in the sense that the magnitude of the gradient term in (2.8) is much smaller than the first term, we can view it as giving a small correction to the force acting on the particle. The ratio between the magnitude of the first and second terms in (2.8) is given by $\epsilon \equiv \rho|\nabla B|/B$, which will be treated as the small parameter in our perturbation expansion, $\epsilon \ll 1$.

To lowest order in ϵ, the particle experiences the force due to a constant magnetic field $\boldsymbol{B} = \boldsymbol{B}(\boldsymbol{X})$, so the lowest order motion of the particle is given by the results of the previous section.

Using the lowest order solution, we can calculate corrections to the particle motion perturbatively. The field felt by the particle along its unperturbed trajectory, $\boldsymbol{x} = \boldsymbol{X}+\boldsymbol{\rho}$, is given by the terms written out in (2.8), which hence are sufficient to calculate the motion to order ϵ.

A subtle issue arises from the fact that we need our approximate solution to be valid for many gyrations. This can be achieved by again considering the motion of the guiding-center rather than that of the particle, and by using a gyroaveraged force [31]. The effective gyroaveraged force felt by the guiding-center due to the first order term in (2.8) is

$$\boldsymbol{F}_{\text{eff}} = \langle e\boldsymbol{v}\times(\boldsymbol{\rho}\cdot\nabla\boldsymbol{B}(\boldsymbol{X}))\rangle_{\boldsymbol{X}}. \tag{2.9}$$

Evaluating this integral gives

$$\boldsymbol{F}_{\text{eff}} = -mv_{\parallel}^2\boldsymbol{\kappa} - \mu\nabla B, \tag{2.10}$$

where $\boldsymbol{\kappa} = -\boldsymbol{b}\times(\nabla\times\boldsymbol{b}) = \boldsymbol{b}\cdot\nabla\boldsymbol{b}$ is the curvature of $\boldsymbol{B}$; $\mu = mv_{\perp}^2/(2B)$ is the magnetic moment. Note that the fields here are evaluated at $\boldsymbol{X}$. The

[1] For deriving the equation of guiding-center motion accurate to arbitrary order, see e.g. Ref. [29] or Ref. [35].

two contributions to the effective force can be interpreted physically as follows: The curvature term can be understood as a centrifugal force due to the local radius of curvature of the magnetic field. The second term can be recognized as the force acting on a current ring with magnetic moment μ.

The fact that our equation of motion remains accurate over many gyrations is closely related to the concept of *adiabatic invariance* [36, 37]. When formulated in a Lagrangian framework, the independence of the gyroaveraged Lagrangian with respect to γ can be used to derive an invariant [38]. This is an adiabatic invariant if it remains approximately constant over long times, even when a small perturbation is added to the averaged system, i.e. the contribution of the small perturbation does not accumulate. Kruskal [31] has shown that for a Hamiltonian system with only periodic solutions, the Poincaré invariant [39] of the unperturbed system over its period becomes an adiabatic invariant. For the perpendicular motion in a constant magnetic field, this invariant is the magnetic moment μ [37].

Since μ is an adiabatic invariant, we can view it as an internal property of the guiding-center, analogous to a particle's spin. Since the particle's kinetic energy can be written as $mv_\parallel^2/2 + \mu B$, we can view $U = \mu B$ as a contribution to an effective potential energy of the guiding center. From this potential, we can calculate a force $\boldsymbol{F} = -\nabla U$, which gives an intuitive derivation of the second term in (2.10). This term is known as the *mirror force*, as it reflects particles with insufficient parallel velocities to overcome the effective potential.

Given the effective force (2.10), a drift-velocity $\boldsymbol{v}_\mathrm{d}$ may be calculated from (2.6). If we now let $\boldsymbol{E} \neq 0$ and assume that $\boldsymbol{E}$ is also approximately constant in the same manner as $\boldsymbol{B}$, the total velocity of the guiding-center becomes

$$\boldsymbol{u} = v_\parallel \boldsymbol{b} + \boldsymbol{v}_\mathrm{d}, \tag{2.11}$$

where $v_\parallel$ evolves according to the parallel component of $\boldsymbol{F} = e\boldsymbol{E} + \boldsymbol{F}_\mathrm{eff}$ and the drift-velocity $\boldsymbol{v}_\mathrm{d}$ is calculated from $\boldsymbol{F}$ and (2.6),

$$\boldsymbol{v}_\mathrm{d} = \frac{\boldsymbol{E} \times \boldsymbol{B}}{B^2} + \frac{v_\perp^2}{2\Omega} \boldsymbol{b} \times \nabla \log B + \frac{v_\parallel^2}{\Omega} \boldsymbol{b} \times \boldsymbol{\kappa}. \tag{2.12}$$

The first term is the $\boldsymbol{E} \times \boldsymbol{B}$ drift, while the last two terms in (2.12) are the *magnetic drifts* associated with the effective force (2.10). The magnetic drifts are small in ϵ since we assume weakly varying fields, while the $\boldsymbol{E} \times \boldsymbol{B}$ drift in principle can be large. However, large $\boldsymbol{E} \times \boldsymbol{B}$ drifts are

typically not encountered in modern tokamaks [29], so we assume that the $\boldsymbol{E} \times \boldsymbol{B}$ drift is also small, and hence the drift motion corresponds to a small correction to the parallel motion.

Nevertheless, to confine particles in approximately constant fields over reactor-relevant time-scales, the extent of both the drift and parallel motion of the guiding-center described above must be restricted to a bounded volume. We will see in the next section that, in a tokamak, the motion of the guiding-center under the action of these drifts is itself periodic in the non-ignorable coordinates. This situation is partly analogous to the constant field case of the previous section – which also displayed periodic motion in the non-ignorable, perpendicular direction – but provides single-particle confinement in all directions due to toroidal symmetry.

2.1.2 Magnetic confinement in tokamaks

In the previous sections, we saw that magnetic fields confine particles in the perpendicular direction, but that field inhomogeneities of larger-than gyroradius scales result in a perpendicular drift $\boldsymbol{v}_\mathrm{d}$. The particle is not confined in the parallel direction.

The lack of confinement in the parallel direction is not a problem if the magnetic field itself is confined to a bounded region in space. For the magnetic field to not vanish at any point on the boundary of this region, the Poincaré-Hopf theorem states that the boundary has to be topologically equivalent to a torus [40, 41].

In this section, we present a toroidal field configuration where the *drift orbits* of the guiding centers are periodic, and hence confined. This configuration will turn out to be the magnetic field of a tokamak.

To describe a toroidal geometry, we introduce a cylindrical coordinate system, $\{Z, R, \varphi\}$, see Figure 2.1. The radial coordinate R describes the distance from the axis of symmetry; Z is a distance along the axis of symmetry; φ is the azimuthal angle. We also define the toroidal coordinate system $\{\varphi, r, \theta\}$ where r is a distance along the minor radius of the torus; θ is a poloidal angle; φ is known as the toroidal angle in this context.

Let us first consider a purely toroidal magnetic field. From Ampere's law, such a field decreases with radius, so the field gradient points inward along R. This results in magnetic drifts (2.12) in the Z direction, with the sign of the drift depending on the particle's charge. If we were to try to confine a plasma with such a field, these drifts would lead to charge

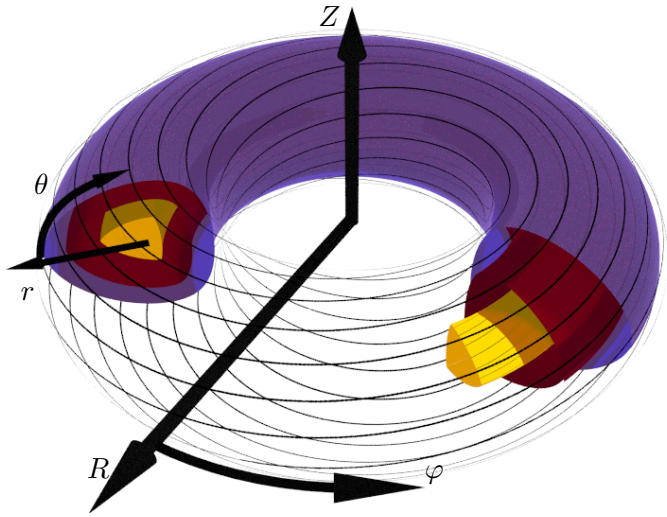

Figure 2.1: A cartoon of a toroidal magnetic field of a tokamak, with a definition of the cylindrical coordinates $\{Z, R, \varphi\}$ and toroidal coordinates $\{\varphi, r, \theta\}$. Nested magnetic surfaces are highlighted for a section of the torus, and a magnetic field-line is depicted in black.

separation, and the resulting electric field would cause the entire plasma to drift outwards in R. A purely toroidal field thus cannot confine a single particle or a plasma.

We can rectify this problem by adding a poloidal component to twist the magnetic field, so that the field-lines are wound helically around nested toroidal surfaces, known as (magnetic) *flux-surfaces*. Such a helical field-line is illustrated by the black curve in Figure 2.1. The only way to produce these field-lines in a toroidally symmetric field is to have a toroidal current in the confined region; this setup is realized in devices known as tokamaks.

To mathematically describe the flux-surfaces, it is convenient to introduce a new radial coordinate, a *flux-surface label* ψ which is constant on a given surface. A common choice for the flux label is to use the *poloidal magnetic flux*

$$\psi = -RA_t, \tag{2.13}$$

where A_t is the toroidal component of the electromagnetic vector-potential $\boldsymbol{A}$, and R is the major radius.

The existence of nested flux surface, combined with toroidal symmetry, can be shown to be a sufficient condition to confine a particle. Due

to toroidal symmetry, the toroidal canonical momentum

$$p_\varphi = Rmv_t + eRA_t = Rmv_t - e\psi, \tag{2.14}$$

must be conserved, by Noether's theorem. Here, v_t is the toroidal component of the velocity. From (2.14) and (2.13), we see that the change in ψ over a particle orbit, $\Delta\psi$, is related to the change in kinetic toroidal angular momentum over charge, $\Delta(Rmv_t/e)$. As conservation of energy implies that the particle cannot gain or lose kinetic momentum indefinitely, this result implies that the particle cannot stray too far from a magnetic surface, and is thus confined.

This confinement is for a single particle. In a plasma, particles will interact with each other, and can thus gain or lose energy and angular momentum. Particle interactions will be the subject of the next section – naively, we can think of the particle interactions as discrete events resulting in the particle taking a step $\Delta\psi$ to a nearby flux-surface. The rate of *collisional transport* will therefore depend on the size of this step. Collisional transport due to deviations $\Delta\psi$ from a flux-surface is known as *neoclassical transport*, to differentiate it from so-called *classical transport*, which is due to the deviations between particles and guiding-center, ρ. As neoclassical transport typically dominates over classical transport, the term is sometimes used synonymously with collisional transport in toroidal magnetic field, which is the sense in which the term is used in the title of this thesis.

We now set out to calculate $\Delta\psi$. However, we first note that (2.14) involves the exact toroidal velocity of the particle – including gyration, which we do not wish to resolve. The contribution from the gyration can be removed by instead considering the motion of the guiding-center. By gyroaveraging the Lagrangian used to derive (2.14), we obtain a Lagrangian for the guiding-center motion [38], at which point Noether's theorem tells us that

$$\langle p_\varphi \rangle_{\boldsymbol{X}} = \frac{RB_t m v_\parallel}{B} - e\psi \tag{2.15}$$

is conserved for the guiding-center motion. As the guiding-center equation of motion remain accurate over reactor-relevant time-scales, (2.15) is also a useful approximate invariant for the particles.

To estimate $\Delta\psi$, we begin by noting that if the first term in (2.15) varies little during an orbit, ψ is approximately constant over the motion of a guiding-center. In this case, we do not expect the values of RB_t and

B to change much over the orbit, so that we can estimate the changes as

$$\Delta\psi = \frac{mRB_t}{eB}\Delta v_\parallel. \tag{2.16}$$

The change in $v_\parallel$ during an orbit can be obtained from the conservation of energy and magnetic moment, and thus depends on the particle's velocity and the magnetic field. We will not specify $\Delta v_\parallel$ so as to remain general, but it can typically be written as v times a factor depending on the magnetic geometry.

The corresponding width in real-space can be obtained by

$$\Delta r \sim \frac{\Delta\psi}{|\nabla\psi|} \sim \frac{mv}{eB_p}\frac{\Delta v_\parallel}{v}, \tag{2.17}$$

where we have used $\boldsymbol{B} = \nabla \times \boldsymbol{A} \implies \nabla\psi = RB_p$, with B_p being the poloidal magnetic field. The condition that B is approximately constant over the orbit can thus be phrased as

$$\frac{\Delta r}{L_B} \sim \frac{mv}{eB_p}\frac{1}{L_B} = \frac{\rho_p}{L_B} \tag{2.18}$$

being small. Here we have defined the *poloidal gyroradius*[2], $\rho_p = mv/(eB_p)$.

With the above results, we are now in a position to revisit the qualitative discussion of (1.2) in the introduction. Comparing (1.2) with (2.8), and identifying $\rho = \Delta r$, we see that the guiding-center formalism is *local*. However, ρ_p can be much larger than ρ if the poloidal field is small, $B_p \ll B$, as in conventional tokamaks. It is thus possible to have situations which are local to a field-line – i.e. when ρ is small and guiding-center motion applies – but still non-local in the radial coordinate ψ due to a large $\Delta r \sim \rho_p$. We will consider such a scenario in chapter 3, where we derive an equation describing the distribution of a large-number of guiding-centers in sharp density and electrostatic potential gradients.

To facilitate this treatment, the next section describes how interactions between the large number of particles in a plasma can be treated statistically.

[2]The fact that the gyroradius involves $v_\perp$ rather than v is often unimportant in a thermalized plasma, as equipartition of energy implies that both $v_\parallel$, $v_\perp$ and v all tend to be comparable to the thermal velocity.

2.2 Kinetic theory and collision operators

In the previous section, we considered the motion of a single charged particle in a magnetic field. In this section, we will account for interactions among the many particles of a fusion plasma.

In a plasma, particles interact with each other through long-range electromagnetic forces. The result is an electromagnetic N-body problem. For a fusion plasma, densities are typically of the order $10^{20}\,\mathrm{m}^{-3}$, which means that N will be a very large number. This makes it practically impossible to solve for the motion of individual particles, as we have done above.

However, because N is so large, we can make use of the machinery of statistical mechanics and consider a smooth distribution function in phase-space, that captures the large-scale behavior of our system.

For a statistical treatment, it is useful to express the N-body problem in terms of a Klimontovich equation

$$\frac{\partial}{\partial t} f_{\text{exact}}(t, \boldsymbol{x}, \boldsymbol{v}) + \boldsymbol{v} \cdot \frac{\partial}{\partial x} f_{\text{exact}}(t, \boldsymbol{x}, \boldsymbol{v}) + \boldsymbol{a} \cdot \frac{\partial}{\partial v} f_{\text{exact}}(t, \boldsymbol{x}, \boldsymbol{v}) = 0, \quad (2.19)$$

where $f_{\text{exact}} = \sum_i^N \delta^3(\boldsymbol{x} - \boldsymbol{x}_i)\delta^3(\boldsymbol{v} - \boldsymbol{v}_i)$, is an exact distribution function for N-point particles, with δ the Dirac delta-function and $\boldsymbol{x}_i$ and $\boldsymbol{v}_i$ the position and velocity of particle i; $\boldsymbol{a}$ is the acceleration at phase-space coordinates $(\boldsymbol{x}, \boldsymbol{v})$ – itself a functional of f_{exact} as the particles generate their own electromagnetic fields.

We can identify the differential operator in the Klimontovich equation as the convective derivative in phase-space $\frac{\mathrm{d}}{\mathrm{d}t} \equiv \frac{\partial}{\partial t} + \sum_{i=1}^{6} \dot{z}_i \frac{\partial}{\partial z_i}$, where $\boldsymbol{z} = \{\boldsymbol{x}, \boldsymbol{v}\}$ denotes the position in 6-dimensional phase-space. With this identification, (2.19) follows directly from Liouville's theorem [42].

The N-particle system can be equivalently expressed in terms of n-body distribution functions through the Bogoliubov–Born–Green–Kirkwood–Yvon (BBGKY) hierarchy [43]. These n-body distribution functions give the joint probability of finding n particles in infinitesimal regions around n given points in phase-space, and are thus smooth functions. The calculation of such probabilities relies on assigning probabilities to appropriate microstates, typically by assuming the ergodic hypothesis to hold. The equation for the n-body function involves the $(n + 1)$-body function, and thus we still have N coupled differential equations, as required for this system to be equivalent to the N-particle problem.

The advantage of the BBGKY hierarchy is that, under certain conditions, it can be truncated to yield an equation for a smooth 1-particle distribution function f. The argument is similar to the multiple time-scale expansion we will perform in the following chapter, and can be sketched as follows:

In the scenario of interest, where collective effects dominate, the dynamics of the $(n > 1)$-body functions is much faster than that of the 1-body function. The 1-body dynamics can then be neglected for the purpose of solving for the $(n > 1)$-body functions – in particular, the 2-body function can be expressed solely in terms of the instantaneous value of the 1-body function. Thus it becomes possible to rewrite the 2-body term in the equation governing the 1-body function f in terms of the 1-body function itself, yielding a single equation for the 1-body probability distribution function known as the *kinetic equation*:

$$\frac{\partial}{\partial t} f(t, \boldsymbol{x}, \boldsymbol{v}) + \boldsymbol{v} \cdot \frac{\partial}{\partial x} f(t, \boldsymbol{x}, \boldsymbol{v}) + \boldsymbol{a} \cdot \frac{\partial}{\partial v} f(t, \boldsymbol{x}, \boldsymbol{v}) = C_a[f]. \tag{2.20}$$

Equation 2.20 has essentially the same form as (2.19), but with f a smooth, macroscopic 1-particle distribution function and with an extra term $C[f]$ which is due to the statistical description of the particle interactions. All many-particle effects depending on the detailed trajectories of the particles are accounted for by a *collision operator* C acting on f.

In general, the plasma consists of more than one species, and we label each species by a subscript. In this case, the collision operator also produces the coupling between species; the net effect on species a from all species is then

$$C[f_a] = \sum_b C_{ab}[f_a, f_b]. \tag{2.21}$$

As (2.20) can be written as $\mathrm{d}f_a/\mathrm{d}t = C[f_a]$, $C[f_a]$ can be interpreted as the rate of change in f_a due to particle interactions.

In magnetic fusion, during normal operation – i.e. not considering runaway phenomena [44] – the dominant interactions are non-relativistic, small-momentum exchange interactions dominated by Coulomb collisions. In this case, C_{ab} is well-approximated by a Fokker-Planck collision operator [45]

$$C_{ab}[f_a, f_b] = \tag{2.22}$$
$$\frac{\ln \Lambda}{8\pi m_a} \frac{e_a^2 e_b^2}{\epsilon_0^2} \frac{\partial}{\partial v_k} \int \frac{u^2 \delta_{kl} - u_k u_l}{u^3} \left[\frac{f_a(\boldsymbol{v})}{m_b} \frac{\partial f_b(\boldsymbol{v}')}{\partial v_l'} - \frac{f_b(\boldsymbol{v}')}{m_a} \frac{\partial f_a(\boldsymbol{v})}{\partial v_l} \right] \mathrm{d}^3 v',$$

where $\boldsymbol{u} = \boldsymbol{v} - \boldsymbol{v}'$ is the relative velocity, δ_{kl} is the Kronecker-delta, summation over repeated indices are implied, and $\ln \Lambda = \ln (12\pi n \lambda_D^3)$ is the Coulomb logarithm, with λ_D the Debye length. With C given by (2.22), the kinetic equation (2.20) is known as the *Fokker-Planck equation*, which is fundamental to many kinetic studies in magnetic fusion.

In the scenario considered above, the condition that "collective-effects dominate" can be conveniently expressed in terms of the number of particles in a sphere of radius λ_D. If this number is much greater than one, a charge in the plasma is effectively screened on distances longer than λ_D, so that the plasma looks neutral on these scales. The distribution functions thus obey the neutrality condition

$$\sum_a Z_a \int \mathrm{d}^3 v \, f_a = 0, \tag{2.23}$$

a result known as *quasi-neutrality*. Here Z_a is the charge of species a given in terms of the elemental charge.

In the next chapter, we will use the Fokker-Planck equation together with our results on single particle motion to derive an equation for the phase-space distribution of guiding-centers in a pedestal – given certain assumptions – and show how this distribution can be used to calculate transport.

Chapter 3

Transport in magnetized plasmas

The kinetic equation derived in the previous section is one of the most fundamental equations in plasma physics. In this chapter, we use the distribution function to calculate the particle, heat and momentum fluxes needed to evaluate the quality of confinement. We first define the fluxes for a generic distribution function. We then give an approximation of the kinetic equation appropriate for describing a magnetized plasma in the absence of rapidly-varying small-amplitude turbulence – the drift-kinetic equation, and simplify the generic expression for the fluxes in terms of solutions to this drift-kinetic equation. Finally, we describe how these solutions are obtained numerically with the PERFECT code.

3.1 Transport moments

From the macroscopic distribution function f, we can calculate any macroscopic plasma quantity by taking velocity moments. Some of the most often used moments are,

$$\text{Density} \qquad n = \int \mathrm{d}^3 v\, f, \tag{3.1}$$

$$\text{Particle flux} \qquad \boldsymbol{\Gamma} = \int \mathrm{d}^3 v\, \boldsymbol{v} f, \tag{3.2}$$

$$\text{Momentum flux} \qquad \vec{\vec{\boldsymbol{\Pi}}} = m \int \mathrm{d}^3 v\, \boldsymbol{v}\boldsymbol{v} f, \tag{3.3}$$

$$\text{Heat flux} \qquad \boldsymbol{Q} = \frac{m}{2} \int \mathrm{d}^3 v\, \boldsymbol{v} v^2 f. \tag{3.4}$$

From the particle flux, we also define the *flow velocity* $\boldsymbol{V} \equiv \boldsymbol{\Gamma}/n$.

Often, a distinction is made between velocity moments taken in the "lab frame" (as above), and moments taken in the frame moving with the plasma fluid-flow velocity $\boldsymbol{v} \to \boldsymbol{v} - \boldsymbol{V}$. The pressure is defined relative to the flow velocity

$$p = \frac{m}{3}\int \mathrm{d}^3v\,(\boldsymbol{v}-\boldsymbol{V})^2 f, \tag{3.5}$$

from which we define the temperature as $T \equiv p/n$. The *conductive heat flux* is defined as

$$\boldsymbol{q} = \frac{m}{2}\int \mathrm{d}^3v\,(\boldsymbol{v}-\boldsymbol{V})|\boldsymbol{v}-\boldsymbol{V}|^2 f. \tag{3.6}$$

which can be related to the heat flux $\boldsymbol{Q}$ by

$$\boldsymbol{q} = \boldsymbol{Q} - \frac{5}{2}p\boldsymbol{V} - \frac{1}{2}nmV^2\boldsymbol{V} - \left(\overleftrightarrow{\boldsymbol{\Pi}}\cdot\boldsymbol{V} - p\boldsymbol{V}\right). \tag{3.7}$$

We will consider scenarios when the flow is small compared to the thermal speed, $v_T \equiv \sqrt{2T/m}$, so the distinction between lab frame and fluid-flow frame is mostly unimportant, except for the heat flux, where the first two terms in (3.7) are comparable in size, so that $\boldsymbol{q}$ is different from $\boldsymbol{Q}$.

The goal of transport theory is often simply to calculate the above moments to evaluate the confinement of particles, momentum and heat. We can get equations directly relating the moments among themselves by taking moments of the kinetic equation (2.20). The first few moments obey:

$$\frac{\partial n}{\partial t} + \nabla\cdot\boldsymbol{\Gamma} = 0 \tag{3.8}$$

$$m\frac{\partial \boldsymbol{\Gamma}}{\partial t} + \nabla\cdot\overleftrightarrow{\boldsymbol{\Pi}} - e\left(n\boldsymbol{E} + \boldsymbol{\Gamma}\times\boldsymbol{B}\right) = \boldsymbol{F}_c \tag{3.9}$$

$$\frac{3}{2}\frac{\partial}{\partial t}\left(p + \frac{mV^2}{2}\right) + \nabla\cdot\boldsymbol{Q} = W_c + e\boldsymbol{\Gamma}\cdot\boldsymbol{E}, \tag{3.10}$$

which describe the conservation of particles, momentum and energy. Here, we have introduced the moments of the collision operator $\boldsymbol{F_c} = \int \mathrm{d}^3v\, m\boldsymbol{v}C[f]$ and $W_c = \int \mathrm{d}^3v\,\frac{m}{2}v^2 C[f]$ – the friction force density and the collisional energy exchange.

The collision operator acts as an effective source-term in (3.9) and (3.10): since the collisions we consider do not convert particles between

different species, there is no source of particles due to collisions. Likewise, since energy and momentum are conserved in each collision, the sum of the friction force and collisional energy exchange over all species is zero. If our plasma is fueled with particles and energy externally – or if fusion reactions occur in our plasma – we add source terms in the kinetic equation, which will contribute to the moment equations above.

The moment equations are more convenient than the kinetic equation, as they are expressed in 3-D real-space – rather than 6-D phase-space – and directly describe the fluxes of particles, momentum, heat, etc. However, they cannot be evaluated without a *closure*.

Specifically, each moment equation in (3.8)–(3.10) couples to higher moment equations, analogously to the n-body distribution functions in the BBGKY hierarchy. Thus we need to evaluate or approximate one of the higher moments to close the set of equations.

A rigorous closure is difficult to find in general. When collisions dominate, i.e. when the plasma is cold, the Chapman-Enskog method can be employed, yielding the Braginskii fluid equations. However, this closure is not applicable to the hundred-million K center of a tokamak plasma, and thus we have to face up to the kinetic equation (2.20). In the following section, we will simplify the kinetic equation in a manner appropriate for quiescent magnetized plasmas, the result of which is the *drift-kinetic equation*. The moment equations can then be used to interpret the moments of the distribution function in (3.1)-(3.6).

3.2 Drift-kinetic equation

In chapter 2, we saw how the motion of particles in magnetic fields that vary weakly over the gyroradius scale can be decomposed into gyration and guiding-center motion. We also saw that the latter was approximately independent of the gyrophase. The same is also true for the distribution function, provided that the gyration is faster than all other time-scales.

To connect our single-particle results to the kinetic description, we first note that its left-hand side of (2.20) is invariant under coordinate transformations on phase-space $\boldsymbol{z} \to \boldsymbol{z}'$, so that we can use *guiding-center coordinates*

$$\boldsymbol{X} = \boldsymbol{x} - \boldsymbol{\rho}, \tag{3.11}$$

where $\boldsymbol{\rho} = \frac{\boldsymbol{b}(\boldsymbol{X})\times\boldsymbol{v}}{\Omega(\boldsymbol{X})}$ is the gyrovector evaluated at $\boldsymbol{X}$. For velocity space, we use the coordinates $\{W, \mu, \gamma\}$, where $W \equiv mv^2/2 + e\Phi$ is the energy of

a particle at point $\boldsymbol{x}, \boldsymbol{v}$ in velocity space, $\mu = mv_\perp^2/(2B)$ is the magnetic moment; γ is an azimuthal angle in velocity space, $\gamma = -\arctan v_2/v_1$. These definitions are essentially the same as in section 2.1, except that $v_\perp$ here is the exact perpendicular velocity, unlike (2.3) and (2.5) which exclude the drifts.

Performing the change of coordinates

$$\{\boldsymbol{x}, \boldsymbol{v}\} \to \{\boldsymbol{X}, W, \mu, \gamma\}, \tag{3.12}$$

the kinetic equation (2.20) becomes

$$\dot{f}_a = \frac{\partial}{\partial t} f_a + \dot{\boldsymbol{X}} \cdot \frac{\partial}{\partial \boldsymbol{X}} f_a + \dot{W} \frac{\partial f}{\partial W} + \dot{\mu} \frac{\partial f}{\partial \mu} + \dot{\gamma} \frac{\partial f}{\partial \gamma} = C[f_a], \tag{3.13}$$

where a dot represents a time derivative along a particle trajectory

$$\dot{A} = \frac{\partial A}{\partial t} + \boldsymbol{v} \cdot \frac{\partial A}{\partial \boldsymbol{x}} + \boldsymbol{a} \cdot \frac{\partial A}{\partial \boldsymbol{v}}, \tag{3.14}$$

with $\boldsymbol{a}$ the acceleration at $\{\boldsymbol{x}, \boldsymbol{v}\}$.

Just as in the single particle case, the guiding-center dynamics will provide a simplification if the gyration perpendicular to the magnetic field-lines dominates over all other time-scales in the equation. When that is the case, (3.13) becomes,

$$\dot{\gamma} \frac{\partial f}{\partial \gamma} = 0, \tag{3.15}$$

which tells us that the distribution function is approximately independent of γ. However, a less crude approximation to the kinetic equation is needed to to find the dependence of f on the other variables.

3.2.1 Approximations and ordering assumptions

To apply a perturbation analysis to the kinetic equation, we need to introduce a formal small parameter ϵ. As in chapter 2, we assume that the magnetic field varies little on the gyroradius-scale, $\epsilon \equiv \rho/L_B \ll 1$, where $L_B = |\nabla \log B|^{-1}$ is the gradient scale-length of B. We here use ρ to denote the thermal gyroradius $\rho = mv_T/(eB)$, which represents a typical gyroradius in our plasma[1]. In this section, we will order the other

[1] This assumes a low flow velocity, so that v_T is representative of a typical particle velocity. The same expansion parameter can also be used in plasma with sonic flows, but the transformation to a frame rotating with the flow velocity introduces some additional terms, see Ref. [46].

Table 3.1: Orderings assumed when deriving the drift-kinetic equation. Definitions of the various quantities are standard and introduced throughout the thesis.

Length-scale of $\boldsymbol{B}$	$L_B \equiv \lvert\nabla \log B\rvert^{-1}$
Expansion parameter	$\epsilon \equiv \rho/L_B \ll 1$
Parallel gradients	$v_\parallel \boldsymbol{b}\cdot\nabla = \mathcal{O}(\epsilon\Omega)$
Perpendicular gradients	$\boldsymbol{v}_\perp \cdot \nabla = \mathcal{O}(\epsilon\Omega)$
Collision operator	$C[f] \sim \nu f = \mathcal{O}(\epsilon\Omega f)$
Parallel electric field	$\frac{e}{m}E_\parallel = \mathcal{O}(\epsilon\Omega v_T)$
Perpendicular electric field	$\frac{e}{m}E_\perp = \mathcal{O}(\epsilon\Omega v_T)$
Time derivatives	$\frac{\partial}{\partial t} = \mathcal{O}(\epsilon^3\Omega)$

quantities in (3.13) in terms of this ϵ. We quantify the statement that gyration dominates other time-scales by ordering the transit frequency $\omega_t = v_T/L_B \sim \epsilon\Omega$, which is the characteristic frequency at which a thermal particle travels a distance on which B may have order unity variations. We also order the effects of collisions, quantified by a collision frequency ν, as $\nu \sim \epsilon\Omega$, and assume that the Lorentz force due to the electric field is weaker than that of the magnetic field $\boldsymbol{E} \sim \epsilon v_T B \sim \epsilon\frac{m}{e}\Omega v_T$. The latter two assumptions can be thought of as a formal definition of what it means for a plasma to be magnetized. We will also assume steady-state, in the sense $\frac{\partial}{\partial t} = \mathcal{O}(\epsilon^3\Omega)$, so that we can neglect all time-derivatives. We summarize these assumptions in Table 3.1.

To relate these orderings to (3.13), we rewrite the velocity-space time-derivatives in terms of the electromagnetic fields [29]

$$\dot{\mu} = -\mu\overbrace{\frac{1}{B}\boldsymbol{v}\cdot\nabla B}^{\epsilon\Omega} - \frac{v_\parallel}{B}\boldsymbol{v}_\perp\cdot\overbrace{(\boldsymbol{v}\cdot\nabla)\boldsymbol{b}}^{\epsilon\Omega} + \overbrace{\frac{e}{mB}\boldsymbol{v}_\perp\cdot\boldsymbol{E}}^{\epsilon\Omega\mu} \tag{3.16}$$

$$\dot{W} = \frac{e}{m}\boldsymbol{v}\cdot\nabla\Phi + \frac{e}{m}\boldsymbol{v}\cdot\boldsymbol{E} = \frac{e}{m}\boldsymbol{v}\cdot\overbrace{\frac{\partial\boldsymbol{A}}{\partial t}}^{\epsilon^3\Omega\boldsymbol{A}} \tag{3.17}$$

$$\dot{\gamma} = \Omega + \frac{v_\parallel}{v_\perp}\hat{\rho}\cdot\overbrace{(\boldsymbol{v}\cdot\nabla)\boldsymbol{b}}^{\epsilon\Omega} + \boldsymbol{e}_3\cdot\overbrace{\dot{\boldsymbol{e}}_2}^{\epsilon\Omega} - \overbrace{\frac{e}{mv_\perp}\hat{\rho}\cdot\boldsymbol{E}}^{\epsilon\Omega}, \tag{3.18}$$

where $\hat{v}_\perp = \boldsymbol{v}_\perp/v_\perp$ and $\hat{\rho} = \boldsymbol{\rho}/\rho$ and the order of the different terms are indicated with an overbrace.

As shown in chapter 2, the velocity of the guiding-center is given by

$$\dot{\boldsymbol{X}} = \overbrace{v_\parallel \boldsymbol{b}}^{\epsilon \Omega L_B} + \overbrace{\frac{\boldsymbol{E}\times\boldsymbol{B}}{B^2}}^{\epsilon^2 \Omega L_B} + \overbrace{\boldsymbol{v}_\mathrm{m}}^{\epsilon^2 \Omega L_B}. \tag{3.19}$$

3.2.2 Hazeltine's recursive drift-kinetic equation

From the orderings of the previous section, one can derive the drift-kinetic equation (DKE). Following Hazeltine's recursive derivation [28, 29] the DKE takes the form

$$(\boldsymbol{v}_\parallel + \boldsymbol{v}_d + \boldsymbol{u}_d)\cdot\nabla\bar{f} + \left.\frac{\mathrm{d}\mu}{\mathrm{d}t}\right|_{gc}\frac{\partial\bar{f}}{\partial\mu} = C[\bar{f}], \tag{3.20}$$

where $\boldsymbol{v}_\mathrm{d}$ is the perpendicular drift-velocity derived in the previous section, $\boldsymbol{u}_d$ is a parallel drift,

$$\left.\frac{\mathrm{d}\mu}{\mathrm{d}t}\right|_{gc} = \frac{v_\parallel \mu B}{\Omega}\boldsymbol{b}\cdot\nabla\left(\frac{v_\parallel \boldsymbol{b}\cdot\nabla\times\boldsymbol{b}}{B}\right), \tag{3.21}$$

is a change in magnetic moment as seen by the guiding-center; $\bar{f}$ is the gyroaveraged distribution keeping the exact particle position fixed, rather than the guiding-center. In (3.20), partial derivatives are taken with $\boldsymbol{x}$, W, μ and γ as coordinates.

From $\bar{f}$, the full distribution function can be obtained as [29]

$$\begin{aligned} f = \bar{f} - \boldsymbol{\rho}\cdot\left[\nabla\bar{f} + e\boldsymbol{b}\times\boldsymbol{v}_\mathrm{d}\frac{\partial\bar{f}}{\partial\mu}\right] \\ + \frac{v_\parallel\mu}{\Omega}\frac{\partial\bar{f}}{\partial\mu}\left[\hat{\rho}\hat{v}_\perp : \nabla\boldsymbol{b} - \frac{1}{2}\boldsymbol{b}\cdot\nabla\times\boldsymbol{b}\right] + \mathcal{O}\left(\epsilon^2\bar{f}\right), \end{aligned} \tag{3.22}$$

where $\hat{\rho}$ and $\hat{v}_\perp$ are the unit vectors in the gyroradius direction and in the $\boldsymbol{v}_\perp$ direction. Solving (3.20) for $\bar{f}$ thus gives the entire distribution function through (3.22).

Equation 3.20 is not derived through a perturbation series, and thus contains terms of different order in $\epsilon = \rho|\nabla\ln B|$; it is accurate to order ϵ but captures some additional $\mathcal{O}\left(\epsilon^2 f\right)$ terms [47].

We will see that the presence of these higher order terms makes (3.20) a convenient starting point for constructing a radially-global, linearized DKE. To linearize the DKE, we introduce a new expansion parameter

$$\delta \equiv \frac{\rho_p}{L_B}, \tag{3.23}$$

where $\rho_p = mv_T/(eB_p)$ here is a thermal orbit width, up to some geometric factors. This expansion parameter represents the smallness of the orbit width compared to variations in the magnetic field. Based on the discussion in section 2.1.2, we are thus in a situation where the single-particle drift-orbits are local. The global effects we will consider are rather due to sharp variations in the distribution function, which we presently consider.

We seek a solution to (3.20) of the form

$$\bar{f} = f_0 + f_1 + \mathcal{O}\left(\delta^2 f_0\right), \tag{3.24}$$

where the subscript here refers to the order in δ: $f_1/f_0 \sim \delta$. To facilitate such a perturbative treatment, we need to order the different terms in (3.20) with respect to δ.

As our expansion parameter obeys $\delta = \epsilon B/B_p$, the terms of a given ϵ order in (3.20) will generally have the same order in δ. However, we will allow the electrostatic potential and f_1 to vary on the orbit-width scale ρ_p in the ψ-direction[2]

$$|\nabla\psi|\frac{\partial\Phi}{\partial\psi} \sim \frac{\Phi}{\rho_p} \sim \frac{\Phi}{\delta L_B}, \tag{3.25}$$

$$|\nabla\psi|\frac{\partial f_1}{\partial\psi} \sim \frac{f_1}{\rho_p} \sim \frac{f_1}{\delta L_B} \sim \frac{f_0}{L_B}. \tag{3.26}$$

As a result, these terms will contribute to lower order in δ than in ϵ, which is why it is convenient to start from an equation of mixed order in ϵ. Note that variations on the ρ_p scale are permitted by the DKE (3.20) provided that $\rho_p \gg \rho$ so that the distribution remains local in gyroradius. Hence we also require that the orbit-width and the gyroradius are well separated, which implies that $B_p/B \ll 1$.

The different terms in (3.20) are thus ordered:

$$\boldsymbol{v}_\mathrm{m} \sim \boldsymbol{u}_\mathrm{d} \sim \delta v_T, \tag{3.27}$$

$$\left.\frac{\mathrm{d}\mu}{\mathrm{d}t}\right|_{gc} \sim \delta\mu v_T/L_\parallel, \tag{3.28}$$

[2]The fact that f_1 is allowed sharp variations in (3.26), but not f_0 will be shown to be related to the validity of the linearization in (3.24): the gradient of f_0 will act as a source for f_1, and thus set the size of f_1. An f_0 varying on the ρ_p scale would cause f_1 to violate $f_1 \sim \delta f_0$ and is thus not allowed.

while the $\boldsymbol{E} \times \boldsymbol{B}$-drift in the θ-direction is an order lower in δ than in ϵ

$$\hat{\theta} \cdot \boldsymbol{v}_{\mathrm{E}0} \sim \hat{\theta} \cdot \boldsymbol{v}_{\parallel}. \tag{3.29}$$

Inserting this into (3.20) we have, to order $\mathcal{O}\left(\delta v_T f / L_B\right)$,

$$\left(\boldsymbol{v}_{\parallel} + \boldsymbol{v}_{\mathrm{E}}\right) \cdot \nabla\theta \frac{\partial f_0}{\partial \theta} = C[f_0]. \tag{3.30}$$

We can solve this by making the ansatz that f_0 is a stationary, flux-surface Maxwell-Boltzmann distribution[3],

$$\begin{aligned} f_M(\psi, W) &= \eta(\psi) \left(\frac{m}{2\pi T(\psi)}\right)^{3/2} \mathrm{e}^{-\frac{W}{T}} \\ &= n \left(\frac{m}{2\pi T(\psi)}\right)^{3/2} \mathrm{e}^{-\frac{mv^2}{2T}}, \end{aligned} \tag{3.31}$$

where n is the density of the Maxwellian, T the temperature and $\eta(\psi) = n\mathrm{e}^{e\Phi/T}$ is the *pseudo-density*, which is more convenient when evaluating derivatives with W held fixed.

The zeroth-order distribution function is thus a flux-function (i.e. constant on a flux-surface) in the sense that ∇f_M is in the $\nabla\psi$ direction. However, these derivatives are taken with W fixed. If Φ varies on a flux-surface, the density n – which is more experimentally accessible than f_M – will also vary. Such variations have been observed experimentally [48], but are not considered here for the sake of simplicity.

Thus, we also expand the potential, and assume it to be a flux-function to zeroth-order

$$\Phi = \Phi_0(\psi) + \Phi_1(\psi, \theta) + \mathcal{O}\left(\delta^2 \Phi_0\right), \tag{3.32}$$

where $\Phi_1 \sim \delta\Phi_0$. To be specific, we will take Φ_0 as the flux-surface average of Φ. Furthermore, we assume that $\partial\Phi_1/\partial\psi \sim \delta \mathrm{d}\Phi_0/\mathrm{d}\psi$, so that Φ_1 does not vary on smaller than ρ_p scales. This is consistent with Φ_1 being set by f_1, a result which prove at the end of this section.

With these definitions, we can eliminate Φ_1 by a change of variables $W \to W_0 = mv^2/2 + e\Phi_0 = W - e\Phi_1 + \mathcal{O}\left(\delta^2\right)$, which implies

$$\nabla f = \nabla|_{W_0} f - \frac{\partial f}{\partial W_0} e \nabla|_{W_0} \Phi_1, \tag{3.33}$$

[3] A general Maxwell-Boltzmann distribution may also contain flow velocity. We will here assume that the flows are in higher order contributions to the distribution, consistent with a low-flow ordering.

where ∇ refers to gradients taken with W fixed, as above, and $\nabla|_{W_0}$ refers to gradients with W_0 fixed.

In (3.30), contributions from the second term on the right-hand side of (3.33) are formally small:

$$-\frac{\partial f_M}{\partial W_0} e\,\nabla|_{W_0}\,\Phi_1 \sim \frac{e\Phi_1}{T}\frac{f_M}{L_B} \sim \delta\frac{f_M}{L_B}, \tag{3.34}$$

where we have assumed $\nabla_\parallel \Phi_1 \sim \Phi_1/L_B$ and used $e\Phi_1/T \sim \delta$, which is a consequence of quasi-neutrality within flux-surfaces. Thus, we can replace W with W_0 in (3.31). Under these assumptions, f_M and n are flux-functions.

To the next order, we have

$$\begin{aligned}&(\boldsymbol{v}_\parallel + \boldsymbol{v}_{\mathrm{E}0})\cdot\nabla\theta\,\frac{\partial f_1}{\partial\theta}\bigg|_{W_0} + \boldsymbol{v}_{\mathrm{m}}\cdot\nabla\psi\,\frac{\partial f_1}{\partial\psi}\bigg|_{W_0} - C_l[f_1]\\ &= -(\boldsymbol{v}_\parallel + \boldsymbol{v}_{\mathrm{E}0} + \boldsymbol{v}_m)\cdot\left(\nabla|_{W_0} f_M - \frac{e f_M}{T}\nabla|_{W_0}\Phi_1\right) + \mathcal{O}\left(\delta^2\right),\end{aligned} \tag{3.35}$$

where $\boldsymbol{v}_{E0} = B^{-1}\boldsymbol{b}\times\nabla\Phi_0$ is the $\boldsymbol{E}\times\boldsymbol{B}$-velocity due to Φ_0; we have retained the drift-terms on the left-hand side due to the sharp ψ-derivatives in f_1 and Φ_0; linearized the collision operator $C[f_1] = C_l[f_1] + \mathcal{O}\left(\delta^2\right)$; and performed the change of coordinates to W_0, where the corrections to the f_1 derivatives are formally small.

We can eliminate the last Φ_1 term by defining the non-adiabatic response g as

$$g = f_1 + \frac{e\Phi_1}{T} f_M. \tag{3.36}$$

Since f_M and T vary slowly and are flux-functions, we have that

$$(\boldsymbol{v}_\parallel + \boldsymbol{v}_{\mathrm{d}0})\cdot\nabla|_{W_0}\left(\frac{e\Phi_1}{T} f_M\right) = \frac{e f_M}{T}(\boldsymbol{v}_\parallel + \boldsymbol{v}_{\mathrm{d}0})\cdot\nabla|_{W_0}\,\Phi_1 + \mathcal{O}\left(\delta^2\right), \tag{3.37}$$

where $\boldsymbol{v}_{\mathrm{d}0}$ is the drift velocity excluding the small contribution from Φ_1. Using (3.37) and $C_l[f_M] = 0$, the equation for g becomes

$$(\boldsymbol{v}_\parallel + \boldsymbol{v}_{\mathrm{d}0})\cdot\nabla|_{W_0}\, g - C[g] = -\boldsymbol{v}_{\mathrm{m}}\cdot\nabla\psi\,\frac{\partial f_M}{\partial\psi}\bigg|_{W_0} + S. \tag{3.38}$$

This is the radially-global, linearized drift-kinetic equation solved in this work. In (3.38), we have allowed for a source term S to this order; in

general, radially-global transport is inconsistent with steady-state assumptions unless sources are included, as we will see in the next section. As the source was added at this order, it does not affect the derivation of (3.38).

A corresponding radially-local equation – appropriate for describing core transport – can be obtained from (3.38) if we do not assume that Φ and g vary on the ρ_p scale. The drift term then becomes higher order in δ, and we have

$$\boldsymbol{v}_{\parallel} \cdot \nabla|_{W_0} g - C[g] = -\boldsymbol{v}_{\mathrm{m}} \cdot \nabla\psi \left.\frac{\partial f_M}{\partial \psi}\right|_{W_0} + S. \tag{3.39}$$

In this equation, there is no $\partial g/\partial\psi$ term: for the purpose of calculating g, ψ merely enters as a parameter, and the equation is thus radially-local; unlike in (3.38) the source term in (3.39) is not needed for consistency.

Another possibility is to retain the strong variations in Φ, but assume that g varies weakly, so that the radial $\boldsymbol{v}_m \cdot \nabla g$ term becomes formally small. This intermediate step between (3.38) and (3.39) has been studied analytically [49–52] and numerically [27], where it was found to yield very different results compared to (3.38), unless the problem is designed to produce slow radial variations in g [27].

The methods used for the numerical solution of (3.38) and (3.39) are briefly described in section 3.3. In the remainder of this section, we will consider two aspects of the above derivation in more detail. To simplify notation, we drop the W_0 subscript on derivatives: all derivatives will be taken with W_0 fixed from now on.

First, we show that $g \sim \delta f_M$. From estimating the size of the terms in (3.38), we have

$$v_T \frac{B_p}{B}\frac{g}{L_B} \sim \frac{v_T^2}{L_B \Omega}\frac{f_M}{L_M} \implies g \sim \rho_p \frac{f_M}{L_M}, \tag{3.40}$$

where L_M is the length-scale of the Maxwellian. If $L_M \sim L_B$, we thus have $g \sim \delta f_M$. As

$$\nabla\psi \left.\frac{\partial f_M}{\partial \psi}\right|_{W_0} = \nabla\psi \left[\frac{\partial \ln \eta}{\partial \psi} + \left(\frac{mW_0}{T} - \frac{3}{2}\right)\frac{\partial \ln T}{\partial \psi}\right] f_M, \tag{3.41}$$

the η or T length-scales must be comparable to L_B, but strong n and Φ gradients are possible.

Note that the n (or η), T and Φ_0 profiles are effectively inputs to the equation for g. If they are chosen appropriately, then Φ_1 can be shown

to be $e\Phi_1/(T) \sim \delta$. Specifically, if we take the zeroth order densities to be quasi-neutral, we can estimate the size of Φ_1 by applying quasi-neutrality to f_1

$$\sum_a \int \mathrm{d}^3 v \left(g_a - \frac{e_a \Phi_1}{T_a} f_{Ma} \right) = 0, \tag{3.42}$$

so that

$$\Phi_1 = \frac{1}{\sum_a \frac{e_a n_a}{T_a}} \sum_a \int \mathrm{d}^3 v \, g_a \implies \frac{e\Phi_1}{T} \sim \frac{g}{f_M} \sim \delta, \tag{3.43}$$

as we assumed in our derivation.

3.2.3 Transport moments revisited

In section 3.1, we introduced physical quantities in terms of moments of f, and derived equations directly describing the evolution of these moments. We now rephrase these results in terms of the g obtained from the global drift-kinetic equation (3.38), before we move on to the numerical calculation of g in the next section.

From the previous section, we have

$$\bar{f} = f_M + f_1 = f_M + g - \frac{e\Phi_1}{T} f_M, \tag{3.44}$$

whereupon (3.22) gives f in terms of f_M and g,

$$\begin{aligned} f =& f_M + g - \frac{e\Phi_1}{T} f_M - \boldsymbol{\rho} \cdot \nabla (f_M + g) \\ & - \boldsymbol{\rho} \cdot \left[e\boldsymbol{b} \times \boldsymbol{v}_{\mathrm{d}0} \frac{\partial g}{\partial \mu} \right] + \mathcal{O}\left(\delta^2 f_M\right). \end{aligned} \tag{3.45}$$

Here, we have used that $\partial f_M / \partial \mu = 0$ and ordered $\boldsymbol{\rho} \cdot \nabla (f_M + g) \sim v_\parallel |\nabla b| / \Omega \sim \delta$, as is appropriate for the global theory.

Note that the $e\boldsymbol{\rho} \cdot \boldsymbol{b} \times \boldsymbol{v}_{\mathrm{m}} \partial g / \partial \mu$ term in (3.45) is formally $\mathcal{O}\left(\delta^3 f_M\right)$, but needs to be retained in the divergence-flux terms ($\nabla \cdot \boldsymbol{\Gamma}$, etc.) in the moment equations (3.8)-(3.10) as it can have strong radial variations through g. This is a general issue in the global theory, where formally small terms may have large radial variations, and thus may need to be retained for the purpose of calculating gradients.

For this reason, it is useful to consider the global fluxes via moment equations derived from the drift-kinetic equation (3.38), as these equations contain the derivatives of g and thus do not neglect any required

small terms. These equations will be used to verify that (3.45) contains all the required small terms.

Taking the density $\left(\int \mathrm{d}^3 v\right)$ moment of (3.38), we find [30]

$$\nabla \cdot \left(\int \mathrm{d}^3 v \, [\boldsymbol{v}_\parallel + \boldsymbol{v}_{\mathrm{d}0}] \bar{f} \right) = \int \mathrm{d}^3 v \, S, \tag{3.46}$$

where $\boldsymbol{v}_{\mathrm{d}0}$ includes the formally small $\boldsymbol{v}_{\mathrm{m}}$ term as its only radial component. If we identify the divergence term in (3.46) as $\nabla \cdot \Gamma$, this equation merely restates particle conservation (3.8) for steady state $\partial n / \partial t = 0$ in terms of the motion of guiding-centers. Similarly, we have the energy and toroidal angular momentum conservation equations

$$\begin{aligned} \nabla \cdot \left(\int \mathrm{d}^3 v \, [\boldsymbol{v}_\parallel + \boldsymbol{v}_{\mathrm{d}0}] \frac{m v^2}{2} \bar{f} \right) + \left(\int \mathrm{d}^3 v \, [\boldsymbol{v}_\parallel + \boldsymbol{v}_{\mathrm{d}0}] \bar{f} \right) \cdot e \nabla \Phi_0 \\ = \int \mathrm{d}^3 v \, \frac{m v^2}{2} S, \end{aligned} \tag{3.47}$$

$$\begin{aligned} \nabla \cdot \left(\int \mathrm{d}^3 v \, [\boldsymbol{v}_\parallel + \boldsymbol{v}_{\mathrm{d}0}] \frac{I m v_\parallel}{B} \bar{f} \right) - e \int \mathrm{d}^3 v \, \bar{f} \boldsymbol{v}_{\mathrm{d}0} \cdot \nabla \psi \\ = \int \mathrm{d}^3 v \, \frac{I m v_\parallel}{B} S. \end{aligned} \tag{3.48}$$

Transport of toroidal angular momentum is of particular importance, as the total kinetic toroidal angular momentum (i.e. summed over all species) is conserved, so that the plasma can only spin up or down by transporting angular momentum, or in the presence of momentum sources. As plasma rotation is an important parameter for the transition into H-mode [53], this can have large implications for the confining properties of a reactor.

The divergence terms in (3.46)-(3.48) practically define the particle, heat and momentum fluxes. As these fluxes contain $\boldsymbol{v}_m$, we are obliged to retain this term in (3.45) to properly conserve particle, toroidal angular momentum and energy. These indirect definitions do however not capture divergence-free contributions to the fluxes. To capture such term, we turn to the basic definition of the fluxes, i.e. (3.3). Using (3.45), the particle flux becomes [29]

$$\boldsymbol{\Gamma} = \int \mathrm{d}^3 v \, \boldsymbol{v} f = \int \mathrm{d}^3 v \, [\boldsymbol{v}_\parallel + \boldsymbol{v}_{\mathrm{d}0}] \bar{f} - \nabla \times \left(\frac{\boldsymbol{b}}{2\Omega} \int \mathrm{d}^3 v \, \bar{f} v_\perp^2 \right), \tag{3.49}$$

which contains an additional divergence-free term compared to (3.46). This term represents the magnetization flow due to the gyration of the

particles around the guiding-centers, given by the $-\boldsymbol{\rho}\cdot\nabla\bar{f}$ term in (3.45). This form of the fluxes is well-known from local theory [29]; the only difference in the global theory is the ordering of specific terms. In particular, Ref. [30] shows that, to $\mathcal{O}(\delta v_T n)$, the sharp ψ gradients in g gives a new contribution to the divergenceless magnetization flux, while the $\boldsymbol{E}\times\boldsymbol{B}$ drift acting on g contributes to the poloidal fluxes.

Although the divergence-free term is of interest for calculating the fluxes within flux-surfaces, it does not directly contribute to the total radial transport – as follows from applying Gauss' theorem to the volume $V(\psi)$ bounded by that flux-surface ψ. Thus, the fluxes as implicitly defined by (3.46)–(3.48) are sufficient for calculating the total radial fluxes.

To calculate the total radial fluxes, we project the fluxes (3.46)–(3.48) onto the radial direction ($\nabla\psi$) and integrate over a flux surfaces. This integral needs to be defined with some care, as a surface is a null-set and thus, for example, contain zero particles. Thus, we define the *flux-surface average* as the average over the volume $\mathrm{d}V$ between two infinitesimally separated flux-surfaces labeled by ψ and $\psi+\mathrm{d}\psi$, which we express mathematically as

$$\langle A\rangle = \frac{1}{dV}\int_{dV} A\,\mathcal{J}\mathrm{d}\psi\mathrm{d}\theta\mathrm{d}\psi = \frac{1}{V'}\oint\oint\frac{A\,\mathrm{d}\theta\mathrm{d}\varphi}{|\boldsymbol{B}\cdot\nabla\theta|} = \frac{2\pi}{V'}\oint\frac{A\,\mathrm{d}\theta}{|\boldsymbol{B}\cdot\nabla\theta|}, \tag{3.50}$$

where $V'=\mathrm{d}V/\mathrm{d}\psi$ and the equalities follow from axisymmetry and identifying $|\boldsymbol{B}\cdot\nabla\theta| = |\nabla\theta\cdot(\nabla\varphi\times\nabla\psi)|$ as the Jacobian of the $\{\varphi,\psi,\theta\}$ coordinates.

The total radial fluxes of particle, energy and toroidal angular momentum through a flux-surface thus become

$$V'\langle\boldsymbol{\Gamma}\cdot\nabla\psi\rangle = V'\left\langle\int\mathrm{d}^3v\,\boldsymbol{v}_m\cdot\nabla\psi g\right\rangle \tag{3.51}$$

$$V'\langle\boldsymbol{Q}\cdot\nabla\psi\rangle = V'\left\langle\int\mathrm{d}^3v\,\boldsymbol{v}_m\cdot\nabla\psi\frac{mv^2}{2}g\right\rangle \tag{3.52}$$

$$V'\langle R\hat{\phi}\cdot\overleftrightarrow{\boldsymbol{\Pi}}\cdot\nabla\psi\rangle = V'\left\langle\int\mathrm{d}^3v\,\boldsymbol{v}_m\cdot\nabla\psi\frac{mIv_\parallel}{B}g\right\rangle. \tag{3.53}$$

Moment equations directly involving these total radial fluxes are obtained by taking the flux-surface average of (3.46)–(3.48), and using the identity

$$\langle\nabla\cdot\boldsymbol{A}\rangle = \frac{1}{V'}\frac{\mathrm{d}}{\mathrm{d}\psi}\left(V'\langle\boldsymbol{A}\cdot\nabla\psi\rangle\right), \tag{3.54}$$

For (3.46), this results in

$$\frac{1}{V'}\frac{\mathrm{d}}{\mathrm{d}\psi}\left(V'\langle\boldsymbol{\Gamma}\cdot\nabla\psi\rangle\right) = \left\langle\int \mathrm{d}^3v\, S\right\rangle. \tag{3.55}$$

This equation tells us that for $V'\langle\boldsymbol{\Gamma}\cdot\nabla\psi\rangle$ to vary radially – which would occur as a consequence of the sharp radial variation we have allowed in g – sources are needed.

Physically, this result means that the sharp gradients observed in the pedestal will drive fluxes that are incompatible with steady-state collisional transport in the absence of sources, which is why we introduced sources in (3.38).

This incompatibility of steady-state assumptions and radially-global transport is also observed in gyrokinetic modeling of plasma turbulence [54], where one typically adds sources either to match physical sources in experiments (referred to as *flux-driven* simulations), or to make the profiles remain close to the experimentally observed profiles (known as *profile-driven* simulations) [55]. The latter approach is used in this work; an argument for this approach can be made as follows:

Experimentally observed steady-state profiles are necessarily consistent with the physical total fluxes and sources. If the modeled fluxes are not consistent, there must be other, unmodeled contributions to the flux such that the total flux respects the conservation laws, i.e., for particles

$$\begin{aligned} &\nabla\cdot(\boldsymbol{\Gamma}+\boldsymbol{\Gamma}_{\text{unmodeled}}) = S_{\text{physical}} \\ \Longrightarrow\ &\nabla\cdot\boldsymbol{\Gamma} = S_{\text{physical}} - \nabla\cdot\boldsymbol{\Gamma}_{\text{unmodeled}} \equiv S_{\text{effective}}, \end{aligned} \tag{3.56}$$

where S_{physical} is the physical source. From this equation, we can define an effective source-term given by the divergence of the unmodeled fluxes combined with the physical source. If the model for $\boldsymbol{\Gamma}$ does not depend on the unmodeled fluxes, solving for the sources needed for a consistent steady-state is equivalent to solving for the physical sources combined with the divergence of the unmodeled fluxes.

We will discuss how the effective sources are solved for in this work in the next section, where we numerically solve (3.38) for both g and S. Regardless of the solution method, a general issue with this approach may be noted, namely that the total flux is not determined. For the radial flux, the situation is illustrated in Figure 3.1 for the case of no physical sources, so that any radial gradient in the modeled radial flux must be balanced by the effective sources, here corresponding to a change in the unmodeled fluxes.

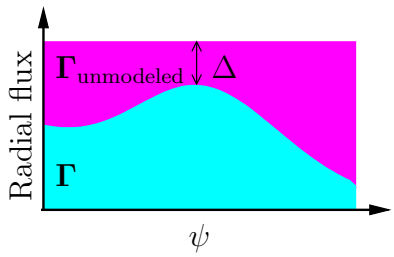

Figure 3.1: Unmodeled and modeled radial steady-state fluxes, for positive unmodeled fluxes and no physical sources. The difference between the maximum of the modeled fluxes and the total fluxes is here indicated by Δ.

As the typical transport in tokamak plasmas is turbulent, a natural candidate for the unmodeled fluxes in our collisional transport model is the turbulent flux. In the pedestal, turbulence is decreased, while the sharp gradients cause the collisional transport to increase, which suggests a picture similar to Figure 3.1. If the unmodeled, radial turbulent fluxes always tend to be positive – as is typically the case for the turbulent heat flux – the peak value of the modeled collisional flux gives the best approximation to the total flux (with the error indicated by Δ in Figure 3.1). Furthermore, if the turbulent flux is small – as is suggested by the sometimes good agreement between collisionally modeled and experimental fluxes [21, 22, 25] – the error in this approximation will be small. Exact estimation of these errors would require radially-global turbulence simulations, which is beyond the scope of this work.

3.3 The PERFECT code

The PERFECT code solves discretized versions of either the local time-independent linearized DKE (3.39) or the global equation (3.38), taking the zeroth order density, temperature and electrostatic potential as inputs and returning (moments of) g and the sources S as outputs.

In the global equation, the sources are solved for alongside g, typically by demanding that the flux-surface averages of the perturbed den-

sity and pressure are zero

$$\begin{aligned} \left\langle \int \mathrm{d}^3 v\, g \right\rangle &= 0, \\ \left\langle \int \mathrm{d}^3 v\, v^2 g \right\rangle &= 0. \end{aligned} \tag{3.57}$$

This provides two ψ-dependent constraints for each species, which allows us to solve for the ψ-dependence of two kinds of sources – typically taken to be heat and particle sources in PERFECT. The velocity and θ dependence of the sources can be specified by the user; the former differentiates particle from heat sources, as specific velocity space-structures only contribute to certain velocity moments. PERFECT allows for flexibility in specifying sources, and (3.57) can be supplemented or replaced with other constraints on g; for simulations with zero radial current, we use an additional unknown momentum source with a prespecified species dependence to balance the additional constraint on the current.

Equation 3.57 also makes it easier to specify the zeroth-order Maxwellian from experimental data, as it implies that the density and temperature in the Maxwellian should correspond to the flux-surface averages of those quantities.

Apart from sources, the solution of the global equation is further complicated by the need to apply radial boundary conditions to the problem. PERFECT has the flexibility to apply three alternative conditions: Dirichlet boundary conditions $g(\psi_1) = g_{\mathrm{local}}(\psi_1)$ or $g(\psi_1) = 0$, or Neumann $\boldsymbol{v}_{\mathrm{d0}} \cdot \nabla g = 0$. These are applied at the boundaries where radially drifting particles enter the domain.

Rather than the W_0 and μ used to derive the DKE in the previous section, PERFECT uses $x = v/v_T$ and $\xi = v_\parallel/v$, which allows for a more convenient representation of the full linearized Fokker-Planck collision operator. The discretization of the problem is done by finite difference in ψ and θ, a Legendre polynomial expansion in ξ and by using spectral collocation in x [27].

With this discretization, the global DKE (3.38) and the constraints (3.57) – and also the local DKE (3.39) without constraints – can be written as a matrix inversion problem. In PERFECT, this problem is solved using PETSc's Krylov solver [56] with preconditioners based on simplified forms of the problem, generated by, for example, dropping off-diagonal terms.

Factorization of the preconditioner matrix is typically the lengthiest part of the computation, and the often large size of the matrix means

that PERFECT needs several hundred gigabytes of memory to solve the global equation at realistic resolutions. Depending on the tolerance requirement of the Krylov solver, numerous Krylov iterations may also be needed to obtain a solution.

Once the distribution is obtained, PERFECT calculates the fluxes described in the previous section as outputs. In the next section, we summarize results obtained by applying PERFECT to various problems related to neoclassical pedestal transport.

Chapter 4

Summary of papers

In the previous chapters, we introduced a theoretical framework for studying neoclassical transport in tokamak pedestals. In this chapter, we give an overview of the work we have done in this framework by summarizing the four attached papers.

In Paper A we looked at changes in transport due to the presence of trace and non-trace nitrogen *impurities* in the pedestal. Impurities are non-fuel plasma species, usually present in small quantities, as a result of plasma-wall interactions, as rest products from fusion ("helium ash"), or due to deliberate injection. Such impurities can be problematic, as they dilute the plasma, and highly-charged species can emit significant electromagnetic radiation at higher temperatures, which represents an irreducible energy loss to terrestrial fusion plasmas.

It is thus important that impurities do not accumulate in the hot core of the plasma. However, impurities can also have beneficial effects. As an example of this, when the tokamak JET[1] switched from a carbon to a beryllium-tungsten ("ITER[2]-like") wall, there was a reduction in energy confinement [57–59]. This decrease in confinement was attributed to a reduction in the impurity content of the plasma as a result of the new wall, and could sometimes be recovered by injecting nitrogen [58, 60].

To study this, we used a set of experimental JET electron profiles (Figure 16 of Ref. [61]), and complemented these with model potential and ion profiles designed to satisfy the assumptions of the global DKE:

[1] **J**oint **E**uropean **T**orus, the world's largest tokamak, hosted in the UK on behalf of EUROfusion.

[2] *ITER*: Latin for "the way", a tokamak currently being built in Cadarache, France, which upon its completion will be the largest tokamak to date.

gentle T_i variations – here based on the core T_e gradients – and electrostatic ion confinement.

As a result of the electron temperature pedestal, large electron particle fluxes developed both in and across flux surfaces. These fluxes were well-described by the local theory, due to the small orbit width of the electrons and the low flow of the ions, which otherwise would affect the electrons through collisions. Thus, the parallel current in these simulations were well-approximated by results from the local theory. This has implications for evaluating the performance of a tokamak reactor, as the poloidal magnetic field – which determines the orbit width – is set by this current. In addition, stronger parallel current can drive so-called peeling-modes unstable, which can drive the plasma away from a stable pedestal configuration and cause large intermittent heat fluxes [61–64].

For bulk and impurity ions, we find order unity modifications to ion heat and particle fluxes due to global effects, with impurity particle fluxes even changing sign compared to the local results. These effects are not restricted to the pedestal region, but due to the radially global nature of these effects, they extend a distance into the near-pedestal core, and this distance appears to scale with the orbit width of the species.

Furthermore, the radial fluxes are not intrinsically ambipolar, which here leads to a non-zero radial current and significant radial flux of toroidal angular momentum, while this transport is zero in the local theory. This current and momentum transport is strongly affected by the nitrogen seeding, which could imply that the confinement improvement due to nitrogen seeding might not be directly related to a reduction in heat-flux, but perhaps due to a more efficient suppression of turbulence.

It should be noted that this radial current must be canceled by a non-neoclassical current contribution for the transport to be compatible with steady-state confinement. This would generate a non-neoclassical momentum transport to cancel the neoclassical one here, unless the non-neoclassical transport channel has momentum sources. In Paper C, we showed that the radial neoclassical current can be replaced with a momentum source to yield non-zero radial momentum fluxes consistent with steady-state, which are qualitatively similar to the momentum fluxes with a radial current.

In Paper B – a short conference contribution – we further quantified the size of the momentum transport by computing a proxy for the effective Prandtl number, which was found to be comparable to the effective Prandtl number due to turbulent transport in the core of JET [65] and

KSTAR[3] [66]. If these results extrapolate to experimental pedestal profiles, where the heat flux can be close to neoclassical values, it could imply that the neoclassical momentum flux may be a dominant transport channel for momentum in the pedestal, so that the momentum flux calculated by PERFECT may be close to the total momentum flux.

In Paper C, we used similar input profiles to study flows in D, He and mixed D-He plasmas. The aim of the study was to investigate whether the He flow is a suitable proxy for the D flow, since the latter is harder to measure in experiments [67]. Specifically, we investigated to which extent flow of He impurities in bulk D plasmas is similar to the D flow, and also if the He flow in bulk He plasma is similar to the D flow in bulk D plasma.

We found that the flow of He impurities in a D bulk plasma can be quite similar to those in a bulk He plasma – i.e. that the species role as bulk or impurity was not the dominant factor in our study. Specifically, the extremum values in outboard ($\theta = 0$) and inboard ($\theta = \pi$) poloidal flows were within 0.3 km/s absolute and 15% relative difference, which is within current experimental uncertainties in flow measurements [68, 69]. Likewise, the extremum values poloidal D flows in the bulk and impurity scenario were within 0.5 km/s of each other.

On the other hand, the difference in poloidal flows between the species were significant, around 10 km/s, which indicates that He flows may not be a suitable proxy for D flows. Despite difference in magnitude, the shape of the D and He flow structures in the radial-poloidal plane were qualitatively similar to each other, if the thermal orbit width of the species is interpreted as setting the radial scale of these structures, and this difference is compensated for.

Furthermore, as the divergence of the radial fluxes can not be neglected in the global theory, there is potential for interactions between radial and poloidal fluxes. As a result, radial-poloidal structures in the particle flux can form near the pedestal. As the fluxes are not divergence free on a flux-surface – as assumed in the local theory – the poloidal flow coefficient[4] is not a flux-function, and can even change sign between inboard and outboard side. Thus, changes in the sign of the poloidal flow on a flux-surface could potentially be a an experimental signature of

[3] **K**orea **S**uperconducting **T**okamak **A**dvanced **R**esearch, a tokamak at the National Fusion Research Institute in Daejeon, South Korea

[4] The poloidal flow coefficient, k_p, is essentially the proportionality coefficient between temperature gradient and poloidal flow V_p, with some additional geometric factors: $V_p = k_p B_p B_t R/(e\langle B^2\rangle)\mathrm{d}T/\mathrm{d}\psi$.

global effects.

In Paper D, we investigated isotopic effects in the pedestal. The isotope effect is a phenomenon where the heat fluxes do not follow the expected mass-scaling from local gyro-Bohm-like predictions [70–73]. The isotope effect is typically seen to be stronger for H-mode plasmas [74, 75], and is thus an interesting topic for radially-global studies. Global effects tend to reduce the heat-flux in the pedestal compared to locally predicted values, and these effects are stronger for heavier isotopes due to their wider orbit-widths.

We also investigated the extent to which global corrections to local results can be predicted by experimentally measurable density pedestal parameters: inverse pedestal width over orbit width, relative pedestal density drop and logarithmic gradient times orbit width. The impact of global effects typically increase with all these parameters, and showed signs of saturation for higher values. For fixed width and density at the last-closed flux-surface, the global conductive and convective heat fluxes become less sensitive to the pedestal gradient as it increases, so that the difference between local and global convective and conductive fluxes even may change sign. The trends for the sum of conductive and convective heat fluxes were in general too complicated to give clear predictions: simple empirical models based on polynomials of low degree gave large residuals (and were thus not included in the published paper).

To summarize: radially global effects can introduce order unity modifications to particle and heat fluxes, which extend into the near-pedestal core; the fluxes are no longer divergence free on flux-surfaces; the transport is not intrinsically ambipolar, and momentum transport appears at lower order and is sensitive to impurities when the current is non-ambipolar.

Topics closely related to the work in Paper A and Paper D are presently being pursued by different task forces at JET in order to prepare JET for the upcoming deuterium-tritium campaign, which in turn will provide vital data for the next step towards fusion: the ITER experiment.

Bibliography

[1]R. Clausius and T. Hirst, *The mechanical theory of heat: with its applications to the steam-engine and to the physical properties of bodies* (J. Van Voorst, 1867).

[2]L. Boltzmann and B. McGuinness, *Theoretical physics and philosophical problems: selected writings*, Vienna Circle Collection (Springer Netherlands, 2012).

[3]W. Huang et al., "The AME2016 atomic mass evaluation (I). evaluation of input data; and adjustment procedures", Chinese Physics C **41**, 030002 (2017).

[4]M. Wang et al., "The AME2016 atomic mass evaluation (II). tables, graphs and references", Chinese Physics C **41**, 030003 (2017).

[5]M. P. Fewell, "The atomic nuclide with the highest mean binding energy", American Journal of Physics **63**, 653–658 (1995).

[6]R. H. Cyburt et al., "Big bang nucleosynthesis: present status", Rev. Mod. Phys. **88**, 015004 (2016).

[7]J. P. Conner, T. W. Bonner, and J. R. Smith, "A study of the $H^3(d,n)He^4$ reaction", Phys. Rev. **88**, 468–473 (1952).

[8]W. R. Arnold et al., "Cross sections for the reactions $D(d,p)T$, $D(d,n)He^3$, $T(d,n)He^4$, and $He^3(d,p)He^4$ below 120 keV", Phys. Rev. **93**, 483–497 (1954).

[9]R. Miller, *An introduction to the physics of intense charged particle beams* (Springer US, 2012).

[10]D. Keefe, "Inertial confinement fusion", Annual Review of Nuclear and Particle Science **32**, 391–441 (1982).

[11]H. Antia, A. Bhatnagar, and P. Ulmschneider, *Lectures on solar physics*, Lecture Notes in Physics (Springer Berlin Heidelberg, 2003).

[12]J. W. Connor and H. R. Wilson, "Survey of theories of anomalous transport", Plasma Physics and Controlled Fusion **36**, 719 (1994).

[13]F. Jenko, W. Dorland, and G. W. Hammett, "Critical gradient formula for toroidal electron temperature gradient modes", Physics of Plasmas **8**, 4096–4104 (2001).

[14]P. Mantica et al., "Experimental study of the ion critical-gradient length and stiffness level and the impact of rotation in the JET tokamak", Phys. Rev. Lett. **102**, 175002 (2009).

[15]R. Balescu, *Aspects of anomalous transport in plasmas*, Series in Plasma Physics (CRC Press, 2005).

[16]F. Wagner et al., "Regime of improved confinement and high beta in neutral-beam-heated divertor discharges of the ASDEX tokamak", Phys. Rev. Lett. **49**, 1408–1412 (1982).

[17]F. Wagner, "A quarter-century of H-mode studies", Plasma Physics and Controlled Fusion **49**, B1 (2007).

[18]F. Wagner et al., "Development of an edge transport barrier at the H-mode transition of ASDEX", Phys. Rev. Lett. **53**, 1453–1456 (1984).

[19]ITER Physics Expert Group on Confinement and Transport, ITER Physics Expert Group on Confinement Modelling and Database, and ITER Physics Basis Editors, "Chapter 2: plasma confinement and transport", Nuclear Fusion **39**, 2175 (1999).

[20]H. Zohm et al., "On the physics guidelines for a tokamak DEMO", Nuclear Fusion **53**, 073019 (2013).

[21]J. Connor et al., "A review of internal transport barrier physics for steady-state operation of tokamaks", Nuclear Fusion **44**, R1 (2004).

[22]H. Urano et al., "Reduced heat transport between edge-localized-mode bursts at low collisionality and small poloidal Larmor radius", Phys. Rev. Lett. **95**, 035003 (2005).

[23]K. D. Marr et al., "Comparison of neoclassical predictions with measured flows and evaluation of a poloidal impurity density asymmetry", Plasma Physics and Controlled Fusion **52**, 055010 (2010).

[24]E. Viezzer et al., "Evidence for the neoclassical nature of the radial electric field in the edge transport barrier of ASDEX Upgrade", Nuclear Fusion **54**, 012003 (2014).

[25]E. Viezzer et al., "Investigation of inter-ELM ion heat transport in the H-mode pedestal of ASDEX Upgrade plasmas", Nuclear Fusion **57**, 022020 (2017).

[26]G. Kagan and P. J. Catto, "Arbitrary poloidal gyroradius effects in tokamak pedestals and transport barriers", Plasma Physics and Controlled Fusion **50**, 085010 (2008).

[27]M. Landreman et al., "Radially global δf computation of neoclassical phenomena in a tokamak pedestal", Plasma Physics and Controlled Fusion **56**, 045005, 045005 (2014).

[28]R. D. Hazeltine, "Recursive derivation of drift-kinetic equation", Plasma Physics **15**, 77 (1973).

[29]R. D. Hazeltine and J. D. Meiss, *Plasma confinement*, Dover Books on Physics (Dover Publications, 2013).

[30]M. Landreman and D. R. Ernst, "Local and global Fokker–Planck neoclassical calculations showing flow and bootstrap current modification in a pedestal", Plasma Physics and Controlled Fusion **54**, 115006 (2012).

[31]M. Kruskal, "Asymptotic theory of hamiltonian and other systems with all solutions nearly periodic", Journal of Mathematical Physics **3**, 806–828 (1962).

[32]A. Baños, "The guiding centre approximation in lowest order", Journal of Plasma Physics **1**, 305–316 (1967).

[33]M. Hoppe, A. Iantchenko, and I. Strandberg, "Simulation of charged particle orbits in fusion plasmas" (Chalmers University of Technology, 2015).

[34]R. Hastie, J. Taylor, and F. Haas, "Adiabatic invariants and the equilibrium of magnetically trapped particles", Annals of Physics **41**, 302–338 (1967).

[35]M. Kruskal, *The gyration of a charged particle*, tech. rep. NYO-7903; PM-S-33 (Project Matterhorn, Princeton University, 1958).

[36]A. Lenard, "Adiabatic invariance to all orders", Annals of Physics **6**, 261–276 (1959).

[37]C. S. Gardner, "Adiabatic invariants of periodic classical systems", Phys. Rev. **115**, 791–794 (1959).

[38]R. G. Littlejohn, "Variational principles of guiding centre motion", Journal of Plasma Physics **29**, 111–125 (1983).

[39]R. D. Hazeltine and F. Waelbroeck, *The framework of plasma physics*, Frontiers in physics (Avalon Publishing, 2004).

[40]H. Hopf, "Abbildungsklassenn-dimensionaler mannigfaltigkeiten", Mathematische Annalen **96**, 209–224 (1927).

[41]M. Hazewinkel, "Poincaré–Hopf theorem", in *Encyclopedia of mathematics* (Kluwer Academic Publishers, 2001).

[42]J. Gibbs, *Elementary principles in statistical mechanics: developed with especial reference to the rational foundations of thermodynamics* (C. Scribner's sons, 1902).

[43]C. Cercignani, V. Gerasimenko, and D. Petrina, *Many-particle dynamics and kinetic equations*, Mathematics and Its Applications (Springer Netherlands, 1997).

[44]O. Embréus, "Kinetic modelling of runaway in plasmas" (Chalmers University of Technology, 2016).

[45]P. Helander and D. Sigmar, *Collisional transport in magnetized plasmas*, Cambridge Monographs on Plasma Physics (Cambridge University Press, 2005).

[46]I. G. Abel et al., "Multiscale gyrokinetics for rotating tokamak plasmas: fluctuations, transport and energy flows", Reports on Progress in Physics **76**, 116201 (2013).

[47]A. N. Simakov and P. J. Catto, "Drift kinetic equation exact through second order in gyroradius expansion", Physics of Plasmas **12**, 012105 (2005).

[48]T. Pütterich et al., "Poloidal asymmetry of parallel rotation measured in ASDEX Upgrade", Nuclear Fusion **52**, 083013 (2012).

[49]I. Pusztai and P. J. Catto, "Neoclassical plateau regime transport in a tokamak pedestal", Plasma Physics and Controlled Fusion **52**, 075016 (2010).

[50]P. J. Catto et al., "A unified treatment of kinetic effects in a tokamak pedestal", Plasma Physics and Controlled Fusion **53**, 054004 (2011).

[51]G. Kagan et al., "Neoclassical theory of pedestal flows and comparison with Alcator C-Mod measurements", Contributions to Plasma Physics **52**, 365–371 (2012).

[52]P. J. Catto et al., "Kinetic effects on a tokamak pedestal ion flow, ion heat transport and bootstrap current", Plasma Physics and Controlled Fusion **55**, 045009 (2013).

[53]P. W. Terry, "Suppression of turbulence and transport by sheared flow", Rev. Mod. Phys. **72**, 109–165 (2000).

[54]Y. Sarazin et al., "Large scale dynamics in flux driven gyrokinetic turbulence", Nuclear Fusion **50**, 054004 (2010).

[55]D. Told, "Gyrokinetic microturbulence in transport barriers" (Universität Ulm, 2012).

[56]S. Balay et al., *PETSc users manual*, tech. rep. ANL-95/11 - Revision 3.6 (Argonne National Laboratory, 2015).

[57]F. Romanelli and JET EFDA Contributors, "Overview of the JET results with the ITER-like wall", Nuclear Fusion **53**, 104002 (2013).

[58]M. N. A. Beurskens et al., "The effect of a metal wall on confinement in JET and ASDEX upgrade", Plasma Physics and Controlled Fusion **55**, 124043 (2013).

[59]M. Beurskens et al., "Global and pedestal confinement in JET with a Be/W metallic wall", Nuclear Fusion **54**, 043001 (2014).

[60]C. Giroud et al., "Impact of nitrogen seeding on confinement and power load control of a high-triangularity JET ELMy H-mode plasma with a metal wall", Nuclear Fusion **53**, 113025 (2013).

[61]C. Maggi et al., "Pedestal confinement and stability in JET-ILW ELMy H-modes", Nuclear Fusion **55**, 113031 (2015).

[62]P. Snyder et al., "A first-principles predictive model of the pedestal height and width: development, testing and ITER optimization with the EPED model", Nuclear Fusion **51**, 103016 (2011).

[63]P. B. Snyder et al., "The EPED pedestal model and edge localized mode-suppressed regimes: studies of quiescent H-mode and development of a model for edge localized mode suppression via resonant magnetic perturbationsa)", Physics of Plasmas **19**, 056115 (2012) http://dx.doi.org/10.1063/1.3699623.

[64]L. Frassinetti et al., "Global and pedestal confinement and pedestal structure in dimensionless collisionality scans of low-triangularity H-mode plasmas in JET-ILW", Nuclear Fusion **57**, 016012 (2017).

[65]T. Tala et al., "Toroidal and poloidal momentum transport studies in JET", Nuclear Fusion **47**, 1012 (2007).

[66]S. H. Ko et al., "Characteristics of toroidal rotation and ion temperature pedestals between ELM bursts in KSTAR H-mode plasmas", Physics of Plasmas **23**, 062502, 062502 (2016).

[67]S. R. Haskey et al., "Measurement of deuterium density profiles in the H-mode steep gradient region using charge exchange recombination spectroscopy on DIII-D", Review of Scientific Instruments **87**, 11E553, 11E553 (2016).

[68]E. Viezzer et al., "Collisionality dependence of edge rotation and in–out impurity asymmetries in ASDEX Upgrade H-mode plasmas", Nuclear Fusion **55**, 123002 (2015).

[69]E. Wolfrum et al., "Overview of recent pedestal studies at ASDEX Upgrade", Nuclear Fusion **55**, 053017 (2015).

[70]M. Bessenrodt-Weberpals et al., "The isotope effect in ASDEX", Nuclear Fusion **33**, 1205 (1993).

[71]S. D. Scott et al., "Isotopic scaling of confinement in deuterium-tritium plasmas", Physics of Plasmas **2**, 2299–2307 (1995).

[72]R. J. Hawryluk, "Results from deuterium-tritium tokamak confinement experiments", Rev. Mod. Phys. **70**, 537–587 (1998).

[73]J. Jacquinot and the JET team, "Deuterium-tritium operation in magnetic confinement experiments: results and underlying physics", Plasma Physics and Controlled Fusion **41**, A13 (1999).

[74]D. Schissel et al., "Energy confinement properties of H-mode discharges in the DIII-D tokamak", Nuclear Fusion **29**, 185 (1989).

[75]J. Jacquinot and the JET team, "Deuterium-tritium operation in magnetic confinement experiments: results and underlying physics", Plasma Physics and Controlled Fusion **41**, A13 (1999).